# PCMD-1 bridges the centrioles and the PCM scaffold in *C. elegans*

Lisa Stenzel[1], Alina Schreiner[1], Elisa Zuccoli[1], Sim Üstüner[1], Judith Mehler[1], Esther Zanin[1,2], Tamara Mikeladze-Dvali[1]*

[1]Department Biology II, Ludwig-Maximilians-University, Munich, 82152 Planegg-Martinsried, Germany
[2] Department Biologie, Friedrich-Alexander-Universität Erlangen-Nürnberg, 91058 Erlangen

*Corresponding author and lead contact: Tamara Mikeladze-Dvali (tmdvali@bio.lmu.de)

## ABSTRACT

Correct cell division relies on the formation of a bipolar spindle. In animal cells, microtubule nucleation at the spindle poles is facilitated by the pericentriolar material (PCM), which assembles around a pair of centrioles. Although centrioles are essential for PCM assembly, proteins that anchor the PCM to the centrioles are less known. Here we investigate the molecular function of PCMD-1 in bridging the PCM and the centrioles in *Caenorhabditis elegans*.
We demonstrate that the centrosomal recruitment of PCMD-1 is dependent on the outer centriolar protein SAS-7. While the most C-terminal part of PCMD-1 is sufficient to target it to the centrosome, the coiled-coil domain promotes its accumulation by facilitating self-interaction. We reveal that PCMD-1 is interacting with the PCM scaffold protein SPD-5, the mitotic kinase PLK-1 and the centriolar protein SAS-4. Using an ectopic translocation assay, we show that PCMD-1 can selectively recruit downstream PCM scaffold components to an ectopic location in the cell, indicating that PCMD-1 is able to anchor the PCM scaffold proteins at the centrioles. Our work suggests that PCMD-1 is an essential functional bridge between the centrioles and the PCM.

## INTRODUCTION

Centrosomes are dynamic, non-membranous organelles that serve as the major microtubule-organizing centers in animal cells and are thus essential for biological processes ranging from polarity establishment to the orchestration of cell division. Centrosomes comprise a centriole pair and the surrounding pericentriolar material (PCM). The PCM dynamically changes in size and material properties during the cell cycle (Woodruff et al., 2015; 2017; Mittasch et al., 2020).
PCM expansion during mitosis facilitates bipolar spindle assembly. At the root of PCM expansion is a proteinaceous matrix that serves as a scaffold for the recruitment of regulatory proteins, including mitotic kinases and microtubule nucleators. In *C. elegans,* this scaffolding function is fulfilled by the self-assembly of the coiled-coil protein SPD-5 (functional homolog of Cdk5Rap2 in humans), which is controlled by phosphorylation through Polo-like kinase PLK-1 (homolog of PLK1 in humans) and the interaction with the coiled-coil protein SPD-2 (homolog of Cep192 in humans) (Hamill et al., 2002; Decker et al., 2011; Woodruff et al., 2015; 2017; Cabral et al., 2019). Our previous findings have revealed

that PCMD-1, a protein with a predicted coiled-coil domain, regulates the spatial integrity of the PCM scaffold, and together with SPD-2, is required for the recruitment of SPD-5 (Erpf et al., 2019). Centrioles serve as condensation centers for PCM proteins. During PCM expansion in mitosis, centrioles contribute to the growth and structural integrity of the PCM scaffold (Cabral et al., 2019). A limited set of centriolar core proteins has been described in *C. elegans* (O'Connell et al., 2001; Kirkham et al., 2003; Leidel and Gönczy, 2003; Dammermann et al., 2004; Delattre et al., 2004; 2006; Kemp et al., 2004; Pelletier et al., 2004; 2006; Leidel et al., 2005; Dammermann et al., 2008; Sugioka et al., 2017). From these proteins, SPD-2, SAS-4 (CPAP homolog) and SAS-7 have been proposed to functionally bridge the PCM and the centrioles (Varadarajan and Rusan, 2018). SAS-4, which localizes to the centrioles and the PCM, plays a critical role in microtubule assembly around the central tube of a forming centriole (Kirkham et al., 2003; Leidel and Gönczy, 2003; Dammermann et al., 2008; Delattre et al., 2006; Pelletier et al., 2006). SAS-7 facilitates the formation of paddlewheel structure on centriolar microtubules and recruits SPD-2, which in turn is needed for centriole duplication and mitotic PCM scaffold expansion (Sugioka et al., 2017).
PCMD-1 is predominantly a centriolar protein, yet its depletion affects SPD-5 recruitment and the structural integrity of the PCM (Erpf et al., 2019), raising the possibility that it functionally connects the PCM scaffold to the centrioles. However, the precise mechanisms of PCMD-1 centriolar targeting and how PCMD-1 recruits PCM components has still to be elucidated. Here we investigate the function of PCMD-1 in functionally bridging centrioles and PCM in *C. elegans* embryos.

## RESULTS

### SAS-7 maintains PCMD-1 at the centrioles in early embryos

PCMD-1 localizes weakly to the PCM and strongly to centrioles. PCMD-1 does not require the PCM scaffold protein SPD-5 for its localization in one-cell embryos (Erpf et al., 2019). This raises the questions of whether PCMD-1 is recruited to the centrosome via outer centriolar proteins and whether PCMD-1, in turn, has a role in maintaining these proteins at centrioles. One candidate for such interaction is SAS-7 needed for the formation of paddlewheels, the outermost centriolar structures known in *C. elegans* (Sugioka et al., 2017). We investigated the spatial relationship between PCMD-1 and SAS-7 by analyzing embryos expressing endogenously tagged GFP::PCMD-1 and RFP::SAS-7 using Lattice Structured Illumination Microscopy (SIM) (Figure 1A). We found that PCMD-1 and SAS-7 signals largely overlapped on both centrioles at spindle poles of mitotic blastomeres in early embryos (Figure 1A). This observation prompted us to test whether SAS-7 and PCMD-1 localization are interdependent. Live-cell imaging of GFP::SAS-7 in the *pcmd-1(t3421)* mutant embryos revealed that GFP::SAS-7 levels at centrioles are comparable to control embryos (Figures 1B, 1C). We concluded that PCMD-1 is not involved in the recruitment of SAS-7 to the centrioles. To test inversely whether SAS-7 is required for PCMD-1 recruitment to the centrosome, we crossed an in locus tagged *gfp::pcmd-1* with *sas-7(or452)* mutant animals. While GFP::PCMD-1 at the centrosome was apparent in all control embryos, the centrosomal GFP::PCMD-1 signal was significantly reduced in *gfp::pcmd-1;sas-7(or452)* one-cell embryos (Figures 1D, 1E). Interestingly, a GFP::PCMD-1 signal was consistently detected at sperm-derived *sas-7(or452)* centrioles during pronuclear migration (Figure S1A). Shortly thereafter, this signal decreased close to the detection limit (Figures 1E, S1A). As an

alternative mean to address the SAS-7-dependent localization of PCMD-1, we performed immunostaining using antibodies against GFP and SAS-4 to mark the centrioles. In one-cell control embryos, all centrosomal SAS-4 foci colocalized with a clear GFP::PCMD-1 signal (Figure 1F). In contrast, only a very weak GFP::PCMD-1 signal was observed at SAS-4 foci in *gfp::pcmd-1;sas-7(or452)* embryos (Figure 1F), probably reflecting the hypomorphic nature of the *sas-7(or452)* allele (Sugioka et al., 2017). Note that centrosomal GFP::PCMD-1 signal was detectable in *sas-7(or452)* multicellular embryos (Figure S1B). In these late embryos, PCMD-1 could be recruited through a SAS-7-independent mechanism, as is the case at the ciliary base (Garbrecht et al., 2021; Magescas et al., 2021). Thus, SAS-7 is necessary to maintain PCMD-1 at the centrosome during the first cell division.

**PCMD-1 bridges centriolar and PCM scaffold proteins**

The genetic dependency of PCMD-1 centrosomal localization on SAS-7 raises the possibility that PCMD-1 is recruited to the centriole by direct interaction with SAS-7. To address if PCMD-1 and SAS-7 interact with each other and with other centrosomal proteins such as SAS-4, SPD-2, SPD-5, and PLK-1, we performed a candidate-based yeast two-hybrid screen (Fields and Song, 1989). We generated bait-plasmids containing the cDNAs of SAS-7 and PCMD-1 and prey-plasmids for the candidate proteins SAS-4, SAS-7, PCMD-1, SPD-2, SPD-5, and PLK-1. The readouts of positive interactions were growth and the expression of a GFP-reporter. We categorize proteins showing both readouts on day 3 as strong interactors and on day 5 as weak interactors.

Previous yeast two-hybrid screens identified SAS-7 as a binding partner of SPD-2 (Sugioka et al., 2017; Boxem et al., 2008; Li et al., 2004) and SAS-4 (Boxem et al., 2008). We used these interactions to validate our yeast two-hybrid assay. As previously reported, we found that SAS-7 interacts with SPD-2 and SAS-4 (Figures 2A, 2B). However, we could not detect an interaction between SAS-7 and PCMD-1 using either protein as bait and prey. Therefore, we tested whether PCMD-1 could interact with the centriolar proteins SAS-4 or SPD-2. We observed strong interaction of PCMD-1 with SAS-4 but not with SPD-2. Next, we tested whether PCMD-1 could bind to the PCM scaffold protein SPD-5, the kinase PLK-1 or itself. We detected strong interaction of PCMD-1 with itself and a weaker interaction with SPD-5 and PLK-1. In turn, SAS-7 did not interact with SPD-5 or with PLK-1 (Figures 2A, 2B).

To confirm the interactions between the PCMD-1 bait and SAS-4, PLK-1 and SPD-5 preys, we reversed bait and prey. Again, we observed that PLK-1 and SAS-4 interacted with PCMD-1 (Figure 2C). Since SPD-5 bait autoactivated (not shown), we turned to an alternative assay to confirm this interaction. We expressed *C. elegans* PCMD-1 tagged with EGFP (EGFP::PCMD-1) and SPD-5 tagged with mCherry and 6xHis (mCherry::SPD-5::6xHIS) in human HEK293T cells and performed a co-immunoprecipitation. We successfully co-immunoprecipitated EGFP::PCMD-1 with SPD-5, confirming our yeast two-hybrid observation (Figure 2D).

The yeast two-hybrid assay revealed no interaction of PCMD-1 with SAS-7 or SPD-2. However, both PCMD-1 and SAS-7 interact with SAS-4. Thus, rather than direct recruitment of PCMD-1 by SPD-2 or SAS-7, SAS-4 could theoretically act as a linker between PCMD-1 and SAS-7. However, in accordance with previous studies we found that in *sas-7(or452)* mutant embryos, where no PCMD-1 is found at the centrosome, SAS-4 foci are still present (Figure 1F) (Sugioka et al., 2017). Therefore, it is highly unlikely that SAS-4 is accountable for the loss of PCMD-1 centrosomal localization in *sas-7(or452)* embryos.

In summary, PCMD-1 interacts with the centriolar protein SAS-4, the PCM protein SPD-5, the mitotic kinase PLK-1, and with itself. We propose that PCMD-1 acts as a functional bridge between the centrioles and the PCM scaffold.

**PCMD-1 recruits SPD-5 and PLK-1 to an ectopic location**

PCMD-1 is required to recruit SPD-5 to the centrosome (Erpf et al., 2019). This finding is strongly supported by our yeast-two hybrid interaction data, which indicates that PCMD-1 anchors the PCM scaffold to the centriole. Therefore, we asked whether PCMD-1 is also able to recruit SPD-5 to an ectopic location. To address this, we established a 'translocation assay' by targeting PCMD-1 to an ectopic location in the cell and testing whether PCMD-1 is capable of recruiting SPD-5 to this cellular location. To tether PCMD-1 to the plasma membrane, we fused the mkate2::PCMD-1 reporter to the plcδ1PH-domain and expressed it under a heat shock promoter. Upon heat shock, PH::mkate2::PCMD-1 was expressed and reliably translocated to the plasma membrane (Figures 3A, 3B).

We tested whether membrane-bound PH::mkate2::PCMD-1 could recruit GFP::SPD-5 in the *pcmd-1(t3421)* mutant, which has a premature stop codon, and in the presence of wild-type PCMD-1. In *pcmd-1(t3421)* animals, recruitment of SPD-5 to the centrosome is compromised due to the lack of endogenous PCMD-1 (Erpf et al., 2019). Therefore, more GFP::SPD-5 is expected in the cytoplasm. In control embryos without heat shock, GFP::SPD-5 was never detected at the plasma membrane. Induction of PH::mkate2::PCMD-1 by heat shock resulted in GFP::SPD-5 localization to the plasma membrane in 95.2% of the *pcmd-1(t3421)* and 68.4% of the wild-type embryos (Figures 3B, 3C, S2A, S2B).

Since PLK-1 is also a PCM component and interacts with PCMD-1 in the yeast two-hybrid assay, we tested if PLK-1::sGFP translocates to the plasma membrane in a PCMD-1-dependent manner. Similar to GFP::SPD-5, PLK-1::sGFP localized to the plasma membrane in 41.4% of *pcmd-1(t3421)* and 26.3% of wild-type embryos after heat shock but not without heat shock (Figures 3B, 3C, Figures S2A, S2B). Note that the PLK-1::sGFP signal at the membrane was much weaker compared to the GFP::SPD-5 signal.

SPD-5 phosphorylation by PLK-1 is essential for PCM maturation (Woodruff et al., 2015). In the absence of PLK-1 phosphorylation at four specific residues, SPD-5 only forms a centrosome core but fails to assemble the mitotic scaffold. Therefore, we tested whether the translocation of SPD-5 to the membrane requires phosphorylation by PLK-1 at these residues. For this we used a strain carrying RNAi-resistant GFP::SPD-5(4A), in which the four PLK-1 phosphorylation sites were substituted by alanines (Woodruff et al., 2015). To eliminate the endogenous SPD-5, embryos were treated with RNAi against *spd-5.* We found that GFP::SPD-5(4A) was still able to translocate efficiently to the membrane (96.8%, Figures 3D, 3E), indicating that the membrane-bound GFP::SPD-5 pool does not resemble the mitotic PCM scaffold of SPD-5. Membrane translocation of PLK-1 could be mediated through SPD-5. To test this possibility, we performed the experiment in *spd-5(RNAi)* background. PLK-1::sGFP recruitment still took place (45.9% Figures 3D, 3E). Thus, PCMD-1 can recruit PLK-1 independently of SPD-5.

Next, we tested whether PCMD-1 can also induce translocation of centriolar proteins. Interestingly, PH::mkate2::PCMD-1 was unable to translocate GFP::SAS-4, GFP::SAS-7 or GFP::PCMD-1 in any of the analyzed *pcmd-1(t3421)* embryos (Figures 3B, 3C). This was unexpected, especially for SAS-4, since the interaction in the yeast two-hybrid assay was very strong. One explanation could be that a centriole tethering of SAS-4 prevents membrane translocation by PCMD-1. To test this hypothesis, we used a GFP::SAS-4

construct that lacks the conserved T complex protein 10 (TCP) domain, needed for its binding to SAS-5 (Cottee et al., 2013). When endogenous SAS-4 is eliminated by RNAi, the RNAi resistant GFP::SAS-4(ΔTCP) protein is not tethered to the centrioles but still localizes to the PCM (Cottee et al., 2013) (Figure S2C). In the translocation assay, PCMD-1 was unable to recruit GFP::SAS-4(ΔTCP) to the membrane (Figures S2C, S2D), raising the possibility that the interaction between SAS-4 and PCMD-1 is not through the PCM pool and may require the local environment at the centrioles. Therefore, the ability of PCMD-1 to ectopically anchor proteins to the plasma membrane is specific to the PCM scaffold protein SPD-5 and PLK-1. Alternatively, the deletion of the TCP domain could compromise the interaction between SAS-4 and PCMD-1.

**PCMD-1 is recruited to the centrioles prior to SPD-5**

Our findings suggest that PCMD-1 could recruit the initial PCM core to the PCM-less sperm centrioles in the *C. elegans* one-cell embryo. Therefore, we asked whether PCMD-1 is loaded onto the sperm centrosomes before SPD-5. In the *C. elegans* zygote, SPD-5 is recruited to the sperm-derived centrioles after the completion of meiosis II of the female pronucleus and concomitant with the ability of the centrosome to nucleate microtubules (McNally et al., 2012). This paradigm allows us to investigate whether PCMD-1 is loaded to the centrioles prior to SPD-5 recruitment using marked mating experiments where only the sperm or the oocyte expresses a fluorescent marker. First, we tested whether paternal GFP::PCMD-1 could be detected at the centrosome after fertilization. For this, we mated *fog-2(q71)* females lacking sperms with GFP::PCMD-1 expressing males, thus labeling sperm centrioles (Figure S3A) (Erpf et al., 2019). We could not detect GFP::PCMD-1 at centrioles in any of the analyzed embryos after the completion of meiosis II. Second, we mated GFP::PCMD-1 females, treated with *fem-1(RNAi)* to block sperm production, with control *fog-2(n71)* males with unlabeled sperm centrioles. We found that the GFP::PCMD-1 signal was detected at the centrosomes in all analyzed embryos during the first mitotic division (Figure S3C). These results suggest that sperm-derived PCMD-1 is not maintained and the maternal PCMD-1 is recruited to the centrioles after fertilization.

To determine when exactly maternal PCMD-1 is recruited to the centriole after fertilization and to temporally map its loading with respect to SPD-5, we immuno-stained embryos from GFP::PCMD-1 females mated with males with unlabeled sperm centrioles (Figures S3C, S3D), using antibodies against SPD-5 and GFP. In meiosis I embryos, neither GFP::PCMD-1 nor SPD-5 foci were present at the centrioles (Figure S3E), indicating that maternal GFP::PCMD-1 was not yet incorporated in the centrioles. During meiosis II we found that a GFP::PCMD-1 focus, without any detectable SPD-5, was visible at 90.5% of sperm centrioles (Figures S3D, S3E). In the remaining 9.5% of embryos, categorized as early meiosis II, neither GFP::PCMD-1 nor SPD-5 foci were present (Figure S3D). Therefore, we conclude that maternal GFP::PCMD-1 is recruited to the sperm centrioles at meiosis II. After meiosis II, when sperm pronuclei are decondensed, SPD-5 colocalized with GFP::PCMD-1 at the centrosomes in 87% of the embryos (Figures S3D, S3E). We never observed embryos with centrosomes only labeled by SPD-5.

In summary, our results are consistent with a model in which maternal GFP::PCMD-1 is recruited to the sperm-derived centrioles shortly after fertilization and subsequently recruits SPD-5 and PLK-1 to form the centrosome core. These findings strengthen the hypothesis that PCMD-1 is bridging centriolar and PCM proteins.

**The coiled-coil domain promotes PCMD-1 loading to the centrosome and self-interaction**

To determine how PCMD-1 is anchored to the centrosome, we next examined which part of the protein is necessary for its centrosomal targeting. PCMD-1 is predicted to have a single coiled-coil domain and six Intrinsically Disordered Regions (IDRs1-6), which partially overlap with low complexity regions (Figure 4A) (UniProt Consortium, 2019; Schultz et al., 2000; Letunic and Bork, 2018). Coiled-coil domains often mediate protein-protein interactions, including oligomerization and these interactions can have regulatory functions for centrosomal proteins (Leidel et al., 2005; Kitagawa et al., 2011; Qiao et al., 2012; Hilbert et al., 2013; Lettman et al., 2013; Rogala et al., 2015). Therefore, we set out to investigate the function of the coiled-coil domain in PCMD-1.

To examine the function of the coiled-coil domain, we deleted the sequence from E86 to and including F118, predicted as the coiled-coil domain by the COILS program (Lupas et al., 1991; Lupas, 1996), using CRISPR/Cas9 in the in locus tagged GFP::PCMD-1 protein. We refer to this deletion as *gfp::pcmd-1(ΔCC)* (Figure 4A). In a lethality test 97.5% of the *gfp::pcmd-1* embryos and 87.6% of the *gfp::pcmd-1(ΔCC)* embryos survived at 25°C (Figure 4B). Thus, the deletion of the predicted coiled-coil domain compromised viability.

Next, we investigated if the GFP::PCMD-1(ΔCC) protein could localize to the centrosome. We performed live-cell imaging on worms expressing GFP::PCMD-1 and GFP::PCMD-1(ΔCC). While GFP::PCMD-1 efficiently localized to the centrosomes in all analyzed embryos, the GFP::PCMD-1(ΔCC) signal on average appeared much weaker (Figure 4C). Measuring the mean centrosomal GFP signal intensity confirmed that PCMD-1 without the coiled-coil domain was significantly reduced at the centrosomes in comparison to wild-type PCMD-1, while cytoplasmic levels remained unchanged (Figures 4D, 4E). Thus, the coiled-coil domain is necessary for efficient centrosomal loading of PCMD-1 but is not essential for the viability of the embryos. Since coiled-coil domains are often implicated in the oligomerization of centrosomal proteins, we asked whether PCMD-1 self-interaction was compromised in the absence of the coiled-coil domain. To this end, we expressed PCMD-1(ΔCC) as a bait plasmid and probed its interaction with the PCMD-1(ΔCC) prey (Figure 4F). In the absence of the coiled-coil domain, PCMD-1 self-interaction was lost (Figure 4F).

This raises the question of how embryos with reduced centrosomal PCMD-1 levels can divide. To investigate whether these animals could still recruit the PCM scaffold, we immuno-stained GFP::PCMD-1(ΔCC) embryos using antibodies against GFP and SPD-5 and performed live-cell imaging of RFP::SPD-5. We found that SPD-5 was still recruited to the centrosome in all analyzed embryos, even in embryos where GFP::PCMD-1(ΔCC) was almost undetectable (Figures 4G, S4A). While overall centrosomal RFP::SPD-5 levels remain similar to the control embryos in the absence of the coiled-coil domain (Figures S4A, S4B), the SPD-5 centrosome matrix appeared to be much more dispersed and disorganized (Figure 4G). To quantify the degree of disorganization, we measured centrosome circularity using immunofluorescent staining. Mean centrosome circularity values significantly drop in *gfp::pcmd-1(ΔCC)* embryos (Figure 4H).

We propose that the coiled-coil domain facilitates PCMD-1 self-interaction and thereby promotes efficient PCMD-1 accumulation at the centrosome and the maintenance of PCM scaffold integrity.

**The regions in the C-terminal part of PCMD-1 target the protein to the centrosome and cilia**

The fact that GFP::PCMD-1(ΔCC) could still be recruited to the centrosome indicates that protein regions other than the coiled-coil domain might play a role in centrosomal anchoring. To map which part of the protein is involved, we used a previously established single copy replacement system (Erpf et al., 2019). *pcmd-1(t3421)* mutant animals carry a stop codon before the coiled-coil domain and are lethal at 25°C (Figure S5A). Reconstituting a single copy of the PCMD-1 cDNA under the regulatory elements of the *mai-2* gene rescue survival rates to 96.2% (Figure S5A). We used this assay to test the functionality and localization of different truncations of the PCMD-1 protein. GFP::PCMD-1(N) spans the region E2-N117, including the first two IDRs and the coiled-coil domain. GFP::PCMD-1(C) comprises amino acids F118 to the stop codon, spanning the remaining IDRs (Figure 5A). In the survival assay GFP::PCMD-1(C) could rescue the lethality of *pcmd-1(t3421)* to 90.8% survival, while GFP::PCMD-1(N) was not sufficient to rescue viability (0.3%) (Figure S5A). Interestingly, GFP::PCMD-1(N) even had a dominant-negative effect on the viability of *pcmd-1(t3421)* at the permissive temperature of 15°C, reducing it from 41% to 28% (Figure S5B).

Next, we assessed the ability of these constructs to localize to the centrosome by live-cell imaging. Centrosomal GFP signal was detected in all GFP::PCMD-1(C) embryos, albeit the GFP signal intensities were slightly reduced compared to control animals (Figures 5B, 5C). In contrast, we could not detect any GFP signal at the centrosome in embryos expressing the GFP::PCMD-1(N) constructs, even though the cytoplasmic levels were much higher (Figures 5B, S5C). Therefore, the C-terminal part of PCMD-1, excluding the coiled-coil domain and the IDR1 and IDR2, is sufficient for PCMD-1 anchoring to the centrosome.

To further map the part of PCMD-1 that targets the protein to the centrosome, we subdivided the C-terminal part into two fragments spanning F118-D342 (C1) and G343-stop codon (C2) (Figure 5A). In the survival assay, neither GFP::PCMD-1(C1) nor GFP::PCMD-1(C2) rescued the lethality of *pcmd-1(t3421)* (Figure S5A). However, GFP::PCMD-1(C2) still localized to the centrosome, while GFP::PCMD-1(C1) did not (Figures 5B, 5C). This raises the possibility that the C2 part of the PCMD-1 could be interacting with SAS-4. Therefore, we expressed the PCMD-1(C2) as a bait together with SAS-4 as a prey in the yeast two-hybrid assay (Figure 5D). The PCMD-1(C2) bait strongly interacted with the SAS-4 prey. A similarly strong interaction was detected between the SAS-4 bait and the PCMD-1(C2) prey (Figure 5D).

Similar to the centrosomes in the embryo, only GFP::PCMD-1, GFP::PCMD-1(C) and GFP::PCMD-1(C2) localized to the ciliary base of adult animals (Figure S6). Especially signals from GFP::PCMD-1(C) and GFP::PCMD-1(C2) appeared stronger than the control, extending along the cilia (Figure S6).

In *pcmd-1(t3421)* mutant animals, SPD-5 recruitment to the centrosome is severely compromised (Erpf et al., 2019). Therefore, we tested whether the truncated parts of PCMD-1 that localize to the centrosome can restore SPD-5 recruitment. In animals expressing GFP::PCMD-1(C), levels of RFP::SPD-5 at metaphase were similar to animals carrying the full-length GFP::PCMD-1. However, in GFP::PCMD-1(C2) expressing animals, RFP::SPD-5 levels were largely reduced (Figures S5C, S5D). Thus, the C2 part of PCMD-1, including the IDR6, is sufficient to target PCMD-1 to the centrosome but is insufficient to recruit the PCM scaffold composed of SPD-5.

The fact that PCMD-1(C2) strongly localizes to the centrosome prompted us to test a construct that lacks the C2 part (GFP::PCMD-1(ΔC2) E2-D342). Surprisingly, GFP::PCMD-1(ΔC2) could still localize to the centrosome, although the centrosomal levels were reduced by 60% in comparison with the full-length construct (Figures 5B, 5C). However, GFP::PCMD-1(ΔC2) fully rescued the viability of *pcmd-1(t3421)* and recruited RFP::SPD-5 to the centrosome (Figures S5A, S5D, S5E).
Intriguingly, we could not detect GFP::PCMD-1(ΔC2) at the cilia, indicating that the C2 part is absolutely essential for ciliary base targeting (Figure S6). Since the C2 part comprises the IDR6, we generated a worm strain that expresses GFP::PCMD-1(ΔC2.2) E2-G514, a construct where the IDR6 is included. Centrosomal GFP::PCMD-1(ΔC2.2) levels were comparable to GFP::PCMD-1(ΔC2), however, the ciliary targeting was restored (Figure S6).
In summary, multiple parts of PCMD-1 contribute to the centrosomal localization of PCMD-1. The PCMD-1(C2) part can bind SAS-4 and is sufficient for anchoring to the centrosome. The N-terminal construct lacking C2 can still localize to the centrosome, suggesting the presence of a second centrosome targeting region. The centrosomal PCMD-1(C2) is insufficient to recruit SPD-5 and for embryonic development. Contrary to this, the N-terminal construct lacking the C2 localizes to the centrosome at largely reduced levels can and restore centrosomal SPD-5 levels and function. The C2 part and specifically the amino acids between D342-G514 encompassing the IDR6 are necessary for cilia localization.

**DISCUSSION**

In this study, we examine the mechanism by which PCMD-1 anchors the PCM scaffold to the centriole. We demonstrate that PCMD-1 interacts with the PCM scaffold protein SPD-5, the mitotic kinase PKL-1 and the centriolar protein SAS-4. Furthermore, tethering PCMD-1 at an ectopic cellular location is sufficient to recruit SPD-5 and PKL-1. In turn, the centrosomal localization of PCMD-1 depends on the outer centriolar protein SAS-7. Together with previous findings that PCMD-1 is required for SPD-5 recruitment to the PCM core in the one-cell embryo, these findings functionally place PCMD-1 between the centrioles and the PCM.

Our analysis revealed that PCMD-1 interacts with SPD-5. A similar protein-protein interaction was established for Pericentrin/PLP, the putative homolog of PCMD-1, and Cdk5rap2/CNN the functional homolog of SPD-5 in vertebrates and *Drosophila,* respectively (Buchman et al., 2010; Lerit et al., 2015; Galletta et al., 2016). The interaction in *C. elegans* is especially important for the initial formation of the PCM core in the one-cell embryo. Paternally contributed centrioles in the one-cell embryo are deficient of the PCM core. SPD-5, which renders the centrioles microtubule-organizing activity, is recruited from the maternal pool after female meiosis (McNally et al., 2012). Our findings that PCMD-1 is associated with centrioles prior to SPD-5 recruitment and that tethering of PCMD-1 at the plasma membrane is sufficient to recruit SPD-5 suggest that PCMD-1 is needed for SPD-5 accumulation and the formation of the PCM core after fertilization. In the translocation assay, PCMD-1 was consistently more powerful to recruit SPD-5 and PLK-1 to the plasma membrane in the absence of an endogenous PCMD-1. In the *pcmd-1(t3421)* mutant background, SPD-5 and PLK-1 are not efficiently recruited to the centrosome and are expected to be more abundant in the cytoplasm. This finding suggests a 'tug-of-war' between the centrosomal and membrane-bound PCMD-1 pools for the recruitment of SPD-5 and PLK-1. Membrane-bound PCMD-1 can also efficiently recruit a phospho-deficient

version of SPD-5 in which the four residues that are phosphorylated by PLK-1 and that are playing a key role in the expansion and maturation of the mitotic PCM scaffold are mutated (Woodruff et al., 2015). Therefore, we speculate that PLK-1 phosphorylation of these residues is not required for PCMD-1 to recruit SPD-5 and the membrane-targeted SPD-5 is analogous to the PCM core. The fact that PLK-1 can be translocated to the membrane in the absence of SPD-5 confirms our previous findings that PCMD-1 contributes to the formation of the PLK-1 pool at the centrosome independently of SPD-5 (Erpf et al., 2019). By bringing together PLK-1 and SPD-5, PCMD-1 facilitates the initiation of the centrosome maturation process.

In contrast to the PCM proteins, PCMD-1 was unable to relocate itself and the centriolar proteins SAS-4 and SAS-7 to the plasma membrane. This is consistent with the observations that the centriolar localization of both SAS-4 and SAS-7 is independent of PCMD-1 (this study and Erpf et al., 2019). At the same time, this is puzzling especially in the case of PCMD-1 and SAS-4, where we found a strong protein-protein interaction in the yeast two-hybrid system. Interactions identified by assays, as the yeast two-hybrid system does not indicate where and when exactly these interactions occur. In the case of PCMD-1, this could be due to a stronger binding of PCMD-1 to other centrosomal proteins, which do not allow for a delocalization.

The fact that PCMD-1 could not recruit SAS-4(ΔTCP) raises the possibility that the PCMD-1/SAS-4 interaction may need a specific local environment or modification, which is provided at the centrioles but is absent at the cytoplasmic pool of the proteins. Since the TCP domain of SAS-4 associates with SAS-5 and the centrioles, SAS-4(ΔTCP) only represents the PCM fraction of SAS-4 (Cottee et al., 2013). Even though we cannot exclude the formal possibility that the deletion of the TCP domain additionally disrupts the interaction with PCMD-1, we consider it highly unlikely. We favor the possibility that either another protein is bridging SAS-4 and PCMD-1 or the proteins are post-translationally modified in the yeast two-hybrid system and at the centrosome, but not on the plasma membrane.

The outer centriolar protein SAS-7 is genetically upstream and required for PCMD-1 centrosomal recruitment in the one-cell embryo. This interaction could be direct or mediated through the known SAS-7 binding partners SPD-2 and SAS-4 (Sugioka et al., 2017). It has been shown previously that SAS-7 is recruiting SPD-2 to the centrosome, in turn, SAS-7 as well as PCMD-1 do not rely on a functional SPD-2 for their centrosomal localization (Sugioka et al., 2017; Erpf et al., 2019). In the yeast two-hybrid assay, PCMD-1 did not interact with SAS-7 or SPD-2. Thus, SPD-2 is an unlikely mediator of this interaction. Since both PCMD-1 and SAS-7 interact with SAS-4 in the yeast two-hybrid assay, one could assume that the interaction is mediated through SAS-4. The absence of a fully formed daughter centriole in *sas-4(RNAi)* embryos does not allow us to make a conclusion about the requirement of SAS-4 for PCMD-1 localization. However, SAS-4 foci are still present in *sas-7(or452)* mutant embryos (Sugioka et al., 2017), where little or no PCMD-1 is found at the centrosome. Although we cannot exclude the formal possibility that in *sas-7(or452)* mutant embryos SAS-4 changes its conformation or lacks a posttranslational modification, which would hinder the interaction with PCMD-1, we do not favor a model where SAS-4 is the only anchor for PCMD-1 on the centriole. We suggest that the interaction between SAS-7 and PCMD-1 is either indirect, through an unknown protein or an additional co-factor or

modification is required for interaction in the yeast two-hybrid and translocation assay. Structurally intact paddlewheels, which are altered in *sas-7(or452)* mutant animals, might be a prerequisite for PCMD-1 anchoring (Sugioka et al., 2017).

The presence of multiple IDRs in PCMD-1 suggests high conformational plasticity of the protein (Uversky, 2019). Our structure-function analysis revealed that multiple regions of PCMD-1 contribute to centrosomal targeting. The PCMD-1(C2) fragment, including the IDR6 is sufficient for the centrosomal localization of PCMD-1. In the yeast two-hybrid assay the same fragment strongly interacts with SAS-4, suggesting an interaction site with the centrioles (Figure 6A). At the same time, centrosomal SPD-5 levels in the PCMD-1(C2) background are highly reduced and are comparable to the *pcmd-1(t3421)* mutants (Erpf et al. 2019). Thus, the PCMD-1(C2) fragment alone is insufficient to recruit SPD-5 and as a result does not support embryonic development. Therefore, we suggest that N-terminal parts of the protein are needed for SPD-5 recruitment and function (Figure 6A). In accordance with this, constructs lacking the C-terminal region (PCMD-1(ΔC2) and PCMD-1(ΔC2.2)), which localize to the centrosome at much-reduced levels, are sufficient to accumulate SPD-5 and sustain viability.
The coiled-coil domain and the IDR1 and IDR2 alone are insufficient for centrosomal targeting. The combination with the adjacent IDRs3-5 restores localization and function. Therefore, the PCMD-1(C1) fragment reconstitutes major functional units. The dominant-negative effect on the viability of the coiled-coil domain and the IDR1 and IDR2 could be explained by a binding or sequestration of PCMD-1 interaction partners. In the context of the full-length protein, the coiled-coil domain significantly contributes to the accumulation of PCMD-1 at the centrosome and is required to form an organized PCM. The fact that the deletion of the coiled-coil domain only partially compromises viability is not surprising since even the complete absence of an expanded SPD-5 scaffold at mitosis does not affect the viability (Woodruff et al., 2015). In animals with the deleted coiled-coil domain, SPD-5 levels are not altered, but the PCM appears more dispersed. This could be a direct effect of the coiled-coil domain on SPD-5 or an indirect effect due to the reduced PCMD-1 levels at the centrosome. In the yeast two-hybrid assay, we identified a strong self-interaction of PCMD-1, pointing to a tendency towards dimerization or formation of higher-order structures. Self-association is frequently found in centrosomal proteins. This has also been demonstrated for PLP in flies (Galletta et al., 2016). The self-interaction is abolished in the absence of the coiled-coil domains in both bait and prey but not when the coiled-coil domain is only deleted in the bait. This might indicate that PCMD-1/PCMD-1 self-interaction is mediated through the binding of the coiled-coiled domain to a different part of the protein, rather than a dimerization of the coiled-coil domain. We speculate that the self-interaction of PCMD-1 plays a significant role in the PCM scaffold integrity. It would be interesting to investigate how exactly the physical properties of the mitotic PCM change in the absence of the coiled-coil domain of PCMD-1.

Recently it was shown that PCMD-1 and SPD-5 play an important role in the function of sensory cilia (Garbrecht et al., 2021; Magescas et al., 2021). After initial recruitment, PCMD-1 and SPD-5 maintain each other at the ciliary base through a positive feedback loop (Garbrecht et al., 2021). Through our structure-function analysis, we could separate the cilia localization of PCMD-1 from the centrosome localization. A part of the C2 region, missing in PCMD-1(ΔC2) but present in PCMD-1(ΔC2.2) restores PCMD-1 at the ciliary base (Figures

S6). Interestingly this region comprises the most C-terminal IDR6 suggesting a potential role in targeting the C2 construct to the cilia. Our observation that PCMD-1 localizes to astral and spindle microtubules (Figure 1A), could indicate a binding to microtubules or a microtubule-binding protein. The enhanced localization of the GFP::PCMD-1(C2) along the length of the cilium may reflect increased microtubule binding, which in the cilia is limited by the N-terminal region in the full-length PCMD-1.

Together we propose a model (Figures 6B, 6C) where PCMD-1 is recruited to the centriole via two anchor points: SAS-7, either directly or indirectly, and SAS-4. The C-terminal part, especially the C2 part of PCMD-1 is sufficient for its centrosomal recruitment and interacts with SAS-4. We speculate that SAS-4 acts in parallel to SAS-7 and that this interaction needs the local environment at the centrioles. Centrosomal PCMD-1 recruits SPD-5 through its N-terminal parts, including the IDRs3-5. By bringing together SPD-5 and PLK-1, PCMD-1 facilitates PCM core formation and PCM maturation. The coiled-coil domain enhances PCMD-1 centrosomal accumulation through its self-interaction and contributes to the stabilization of the mitotic PCM scaffold. Given that proteins other than PCMD-1 as SPD-2 play a role in SPD-5 scaffold formation during mitosis, this model might be cell-cycle specific or needed for the initial recruitment of SPD-5 to the PCM core. In summary, we propose that PCMD-1 is one of the proteins that anchors the PCM to the centrioles and functionally bridges the two centrosomal components.

## METHODS

*C. elegans* strains maintenance

Worms were maintained on NGM plates seeded with the OP50 *E. coli* strain under standard conditions at 15°C (Brenner, 1974). Unless indicated otherwise, for experimental use, progeny of worms shifted to 25°C in L4 stage for 16-20h, was analyzed. *gfp::pcmd-1; sas-7(or452)/hT2* worms were allowed to lay eggs for 3h at 25°C. The laid eggs developed into adults at 25°C for 68h. Progeny of *gfp::pcmd-1;sas-7(or452)* worms were used for further analysis.

Worm strain generation

Worms carrying single-copy transgene insertions were generated by the Universal MosSCI system, according to (Frøkjær-Jensen et al., 2008). Transgenes with the pCFJ350 backbone were injected into EG6699 or EG8081 and the progeny was selected using selection markers. Insertions were verified by PCR. Multiple independent insertion lines were screened for expression of the transgenes.

The *pcmd-1(syb1285 syb486[gfp::pcmd-1(ΔCC)])I* allele was generated by SunyBiotech by deleting 33 amino acids from E86 including F118, spanning the coiled-coil domain ranging from amino acid E86-N117, predicted by COILS program (see below). The deletion was verified by PCR amplification using the oligos gcgctccgttgagaatctcgta and cacaaacgagcccgcacgga and sequencing.

Protein domain prediction and illustration

Intrinsically disordered regions were annotated based on information provided by the UniProt Consortium (UniProt Consortium, 2019). The coiled-coil domain was defined via the COILS program with a 28-residue window comparing both MTK and MTIDK matrices (weighted and unweighted) (Lupas et al., 1991; Lupas, 1996). The domain structures were illustrated using DOG2.0 (Ren et al., 2009).

Yeast strains, media and transformation

Growth and genetic manipulation of the *Saccharomyces cerevisiae* strain EGY 48/194 (MATα, trp 1, his 3, ura 3, leu2::2/4 LECAop-LEU2) were performed using standard genetic techniques. The yeast strain was transformed with plasmids using lithium acetate (1M). The selection of the different plasmids was conducted with complete minimal medium lacking histidine/uracil/tryptophane/leucine. Yeast two-hybrid assays were performed using the Grow'N'Glow GFP Yeast Two-Hybrid System (Mobitech GmbH) according to the manufacturer's protocol. Full-length cDNA of *C. elegans* SAS-7, PCMD-1, PCMD-1(ΔCC), PCMD-1(C2), SPD-5, PLK-1 and SAS-4 were inserted into the bait vector pEG202 containing the DNA binding domain LexA. pEG202_SPD-5 could not be used due to autoactivation. The cDNA of the different candidates PCMD-1, PCMD-1(ΔCC), PCMD-1(C2), SPD-2, SPD-5, PLK-1, SAS-7 and SAS-4 were cloned into the prey vector pJG45 comprising the B42 transcription activation domain. The third plasmid transformed into the yeast was pGNG1-GFP containing the reporter gene *gfp*. pEG202-p53 with pJG45-LTA was used as a positive control, whereas pJG45 without an insert was used as a negative control. The presence of the plasmids in yeast was verified by plasmid extraction, followed by PCR amplification of the inserts and sequencing. The expression of the prey proteins was verified by immunoblotting against an HA-tag.

Cell Lines and Culture Conditions

Human embryonic kidney (HEK) 293T cells were cultured at 37 °C (5% $CO_2$) in Dulbecco's modified Eagle's medium (DMEM) supplemented with 10% fetal bovine serum (FBS, Biochrom), 100 units/mL penicillin and 100 µg/mL streptomycin (Gibco).

Co-Immunoprecipitation

HEK293T cells were transfected with 4 µg DNA of pTMD143 and/or pTMD144. After 24 hours cells were chilled to 4 °C. To prepare cell extracts, cells were washed once with 1xPBS and pelleted by centrifugation at 1 000 g for 5 min. Cell pellets were lysed using 100 µl lysis buffer (10 mM Tris-HCl (pH8.0), 50 mM NaF, 0.3 mM $Na_3VO_4$, 10 mM sodium pyrophosphate, 5 mM ß-glycerolphosphate, 120 mM NaCl, 0.25% NP40) containing protease and phosphatase inhibitors (PhosSTOP, Pefabloc, cOmplete Mini, Pepstatin A, Leupeptin Sigma-Aldrich; Aprotinin, Roth) by incubating them 30 min at 4 °C. Crude extracts were clarified by centrifugation at 4 °C and incubated with RFP-trap agarose beads (ChromoTek). Beads were pre-blocked in 3% BSA and washed 3 x in 500 µl lysis buffer before usage. Beads were then collected by centrifugation at 4°C, washed 1x in lysis buffer and resuspended in SDS gel loading buffer. The double volume was loaded for the CoIP compared to I and FT. Immunoblotting was performed by using a primary antibody mouse 1:1000 α-GFP (Sigma-Aldrich)/ 1:1000 α-His (Thermo Scientific) and HRP-linked anti-mouse secondary antibody (1:7500, Goat Anti-Mouse IgG (H+L)-HRP Conjugate (Bio-Rad)) and detected using the ECL Prime Western Blotting Detection Reagent (Amersham).

Translocation assay

L4 stage worms of different strains carrying the construct with the heat shock promoter (TMD151, TMD157, TMD158, TMD159, TMD162, TMD165, TMD168, TMD167, TMD183 and TMD184) were shifted to 25°C for 15h. Subsequently, worms laid eggs for two hours at 25°C. The embryos were mounted on a 2% agarose pad and heat-shocked at 30°C for 1h (Thermocycler Bio-Rad). After 2h recovery at 20°C, embryos were imaged at a SP5 Leica confocal microscope (see microscopy). Control embryos were incubated at 20°C without heat shock. Feeding RNAi against *spd-5* was performed for 20h at 25°C by using I-2G08 for TMD168 and the pTMD118 feeding clone constructed against the reencoded region (Woodruff et al., 2015; 2017; Mittasch et al., 2020) for TMD151 and TMD162. Soaking RNAi against *sas-4* for TMD183 and TMD184 was performed against the reencoded region (Cottee et al., 2013). dsRNA was made using the MEGAscript T7 Kit (Invitrogen) and primers taatacgactcactatagatggcttccgatgaaaatatcggtgc and taatacgactcactataggcagcgtgctgtccactgtggc. Worms were incubated in 1 µg/µl dsRNA for 48h at 20°C and recovered 24h at 25°C. Both RNAi treatments were validated on N2 worms by lethality tests and DIC imaging. Embryos with a minimum of two cells in case of a weak GFP signal or one cell with the GFP signal surrounding the whole circumference of this cell were considered as positive.

Marked mating experiments

To mark the sperm centrioles in marked mating experiments *fog-2(q71),* females were mated with TMD119 males at 20°C and the progeny imaged by 4D-microscopy. For the converse experiment, TMD119 L4 worms were fed *fem-1(RNAi)* overnight. The hatched progeny was raised on *fem-1(RNAi)* to block sperm production. Feminized animals were mated with *fog-2(q71)* males at 20°C. Progeny of the crosses was either imaged with 4D-microscopy or used for indirect immunofluorescence. Meiotic stages of embryos in fixed samples were staged by the condensation state of the female DNA and the presence of the polar bodies.

Indirect immunofluorescence

Indirect immunofluorescence was performed using a protocol by (Delattre et al., 2004). Hermaphrodite worms were cut in M9 buffer, covered with a coverslip, and placed on ice blocks. After freeze-cracking, slides were fixed in methanol, followed by incubation with primary antibodies anti-SAS-4 (1:500, Santa Cruz Biotechnology), anti-SPD-5 (1:1000, a generous gift from B. Bowerman, (Hamill et al., 2002) and anti-GFP (1:500, Roche) overnight at 4°C and with secondary antibodies Alexa488 (1:500, Invitrogen Molecular Probes), Alexa568 (1:500, Invitrogen Molecular Probes) and Hoechst 33258 (1:1000, Sigma) at room temperature for one hour.

Microscopy

Embryos treated for the translocation assay and indirect immunofluorescence samples were imaged with a resolution of 1024x1024 pixels with HCX PL APO Lambda Blue 63x 1.4 oil objective and a step size of 0.7 µm at a SP5 Leica confocal microscope using the LAS software. For live-cell imaging young adult worms were either dissected in 6 µl M9 and mounted on 2% agar pads or dissected in Polybead® Microspheres 20.00 µm (diluted 1:10 in M9). Live-cell imaging was performed on an inverted Nikon Eclipse Ti spinning disc confocal microscope using an Andor DU-888 X-11056 camera (1024×1024 pixels), a 100×1.45-NA

Plan-Apochromat oil immersion objective and controlled by the NIS Elements 4.51 software. Z-stacks were taken every 30 s with a step size of 0.7 µm and with 2x2 binning. Embryos for marked mating experiments were imaged at the Zeiss Axio Imager.M2 equipped with epifluorescence and the Time to Live software from Caenotec. Differential interference contrast (DIC) 25 Z-stacks were taken throughout the volume of the embryo every 35 s, fluorescent scans were taken at required time points.
For structured illumination microscopy (SIM) of live *C. elegans* embryos, we used the ZEISS Elyra 7 system in the Lattice SIM mode equipped with a Plan Apochromat 63x/1.40 oil immersion objective. Images were acquired with two pco.edge sCMOS 4.2 cameras simultaneously, using the ZEISS DuoLink adapter. Acquired Z-stacks with a voxel size of 63x63x110 $nm^3$ and FOV size of 1024x1024 pixels were processed using the SIM processing algorithm of ZEN Black 3.0 software. SIM processed Z-stacks have a voxel size of 31.5x31.5x110 $nm^3$. Yeast colonies were acquired using a Leica Stereomicroscope M205 FA, controlled by the Leica Application Suite software (3.2.0.9652) and equipped with a 1x 2.11 NA Plan Apo lens and a Leica DigitalDFC340x FX camera.

Fluorescent intensity measurements

GFP and RFP intensities were measured on raw images by analyzing Z-stacks with ManualTrackMate in Fiji (Tinevez et al., 2017). The time point was either defined through the DNA condensation visualized by the mCherry::H2B marker (for EU3000, TMD107, TMD165, TMD166, TMD175, TMD177, TMD181, TMD202, TMD210) or through corresponding DIC recordings (for TMD119, TMD123, PHX1285, TMD178, TMD179, TMD203, TMD214, TMD216, TMD217). When there was no clear GFP signal recognizable, the centrosomal position was determined by DIC. A fixed radius was applied to measure all fluorescent signals (GFP::PCMD-1: 0.762 µm for Figure 1E and 0.788 µm for all other figures, GFP::SAS-7: 0.828 µm, RFP::SPD-5: 4.062 µm), background signal, and cytoplasmic background signal outside the embryo, in 3D. Intensities were calculated for each centrosome: intensity = (C-B) – (CS-B). The total intensity of the background (B) was subtracted from the total intensity of the centrosome (C) and from the total intensity of the cytoplasmic signal (CS). The cytoplasmic signal without background was then subtracted from the centrosomal signal without background. For GFP::SAS-7 the sum of the centrosomal fluorescence intensities per embryo was used to calculate the mean centrosomal fluorescence intensities because of separation defects in some *pcmd-1(t3421)* embryos. For cytoplasmic GFP values, the background (B) was subtracted from the cytoplasmic signal (CS).
Statistical analysis was performed by using R Studio version 1.2.5003 (R Core Team, 2014). Shapiro-Wilk test was used to test for normality. Levene's test was performed to compare variances. Dependent on the normality, variance, and number of groups in the data sets, different comparison tests were performed (see Figure legend). Mean values with the standard error of mean were plotted in Prism v6.

Circularity measurements

Centrosomal circularities were evaluated in one-cell embryos ranging from NEB to metaphase that were immunostained with an antibody against SPD-5. The cell stage was defined by DNA condensation, visualized with Hoechst staining. Image analysis was performed in Fiji (Schindelin et al., 2012). Maximum Z-projections were created and the PCM shapes were converted into black/white outlines using the 'Huang' threshold.

Statistical analysis was performed by using R Studio version 1.2.5003 (R Core Team, 2014). Shapiro-Wilk test was used to test for normality. Levene's test was performed to compare variances. Mann-Whitney-U Test was used for the comparison of circularity values. Mean values with the standard error of mean were plotted with Prism v6.

Statistical analysis for survival
L4 worms were singled and maintained at the indicated temperature for 16-20h; laid eggs and hatched adult worms were counted. Statistical analysis was performed in R Studio version 1.2.5003 (R Core Team, 2014). Shapiro-Wilk test was used to test for normality. Levene's test was used to test for homogeneity of variances. Dependent on the normality, variance, and number of groups in the data sets, different comparison tests were performed (see Figure legend).

**ACKNOWLEDGMENTS**

We thank the laboratories of C. Osman and N. Wagener for help with the yeast two-hybrid experiments; the laboratory of A. Böttger for help with the cell culture; M. Antoniolli, N. Sharma, A. Trinca and M. Plotnikova for generating tools; A. Bezler for critical comments on the manuscript; the imaging facility CALM, especially H. Harz and J. Ryan for help with imaging, the whole Zeiss-team and especially M. Gorelashvili for giving us the opportunity to image using the Lattice SIM; N. Lebedeva and M. Nöcker for excellent technical assistance, P. Gönczy, K. Oegema and J. Feldman for providing worm strains, B. Bowerman for the anti-SPD-5 antibody, the LSM graduate school. Some strains used in this study were provided by the Caenorhabditis Genetic Center (CGC), which is funded by the NIH Office of Research Infrastructure Programs (P40 OD010440). The work was funded by the Deutsche Forschungsgemeinschaft: TMD (DFG MI 1867/3) and EZa (ZA/619/3).

**COMPETING INTERESTS**
The authors declare no competing or financial interests.

**AUTHORS CONTRIBUTION**

Experimental design, Methodology – TMD, LS, AS, EZa; Resources, Investigation – LS, AS, EZu, SÜ, JM, TMD; Validation, Formal analysis, Visualization – LS, AS, EZu, TMD; Supervision, Writing – original draft preparation – LS, TMD; Writing – review and editing – TMD, EZa, LS, AS, EZu; Conceptualization - TMD, EZa; Project administration, Funding acquisition -TMD.

**REFERENCES**


Boxem, M., Z. Maliga, N. Klitgord, N. Li, I. Lemmens, M. Mana, L. de Lichtervelde, J.D. Mul, D. van de Peut, M. Devos, N. Simonis, M.A. Yildirim, M. Cokol, H.-L. Kao, A.-S. de Smet, H. Wang, A.-L. Schlaitz, T. Hao, S. Milstein, C. Fan, M. Tipsword, K. Drew, M. Galli, K. Rhrissorrakrai, D. Drechsel, D. Koller, F.P. Roth, L.M. Iakoucheva, A.K. Dunker, R. Bonneau, K.C. Gunsalus, D.E. Hill, F. Piano, J. Tavernier, S. van den Heuvel, A.A. Hyman, and M. Vidal. 2008. A Protein Domain-Based Interactome Network for *C. elegans* Early Embryogenesis. *Cell*. 134:534–545. doi:10.1016/j.cell.2008.07.009.

Brenner, S. 1974. The genetics of *Caenorhabditis elegans*. *Genetics*. 77:71–94.

Buchman, J.J., H.-C. Tseng, Y. Zhou, C.L. Frank, Z. Xie, and L.-H. Tsai. 2010. Cdk5rap2 Interacts with Pericentrin to Maintain the Neural Progenitor Pool in the Developing Neocortex. *Neuron*. 66:386–402. doi:10.1016/j.neuron.2010.03.036.

Cabral, G., T. Laos, J. Dumont, and A. Dammermann. 2019. Differential Requirements for Centrioles in Mitotic Centrosome Growth and Maintenance. *Developmental Cell*. 1–34. doi:10.1016/j.devcel.2019.06.004.

Cottee, M.A., N. Muschalik, Y.L. Wong, C.M. Johnson, S. Johnson, A. Andreeva, K. Oegema, S.M. Lea, J.W. Raff, and M. van Breugel. 2013. Crystal structures of the CPAP/STIL complex reveal its role in centriole assembly and human microcephaly. *eLife*. 2:30–23. doi:10.7554/eLife.01071.

Dammermann, A., P.S. Maddox, A. Desai, and K. Oegema. 2008. SAS-4 is recruited to a dynamic structure in newly forming centrioles that is stabilized by the gamma-tubulin-mediated addition of centriolar microtubules. *The Journal of Cell Biology*. 180:771–785. doi:10.1083/jcb.200709102.

Dammermann, A., T. Müller-Reichert, L. Pelletier, B. Habermann, A. Desai, and K. Oegema. 2004. Centriole Assembly Requires Both Centriolar and Pericentriolar Material Proteins. *Developmental Cell*. 7:815–829. doi:10.1016/j.devcel.2004.10.015.

Decker, M., S. Jaensch, A. Pozniakovsky, A. Zinke, K.F. O'Connell, W. Zachariae, E. Myers, and A.A. Hyman. 2011. Limiting Amounts of Centrosome Material Set Centrosome Size in *C. elegans* Embryos. *Current Biology*. 21:1259–1267. doi:10.1016/j.cub.2011.06.002.

Delattre, M., C. Canard, and P. Gönczy. 2006. Sequential Protein Recruitment in *C. elegans* Centriole Formation. *Current Biology*. 16:1844–1849. doi:10.1016/j.cub.2006.07.059.

Delattre, M., S. Leidel, K. Wani, K. Baumer, J. Bamat, H. Schnabel, R. Feichtinger, R. Schnabel, and P. Gönczy. 2004. Centriolar SAS-5 is required for centrosome duplication in *C. elegans*. *Nature Cell Biology*. 6:656–664. doi:10.1038/ncb1146.

Erpf, A.C., L. Stenzel, N. Memar, M. Antoniolli, M. Osepashvili, R. Schnabel, B. Conradt, and T. Mikeladze-Dvali. 2019. PCMD-1 Organizes Centrosome Matrix Assembly in *C. elegans*. *Current Biology*. 29:1324–1336.e6. doi:10.1016/j.cub.2019.03.029.

Fields, S., and O. Song. 1989. A novel genetic system to detect protein-protein interactions. *Nature*. 340:245–246. doi:10.1038/340245a0.

Frøkjær-Jensen, C., M.W. Davis, C.E. Hopkins, B.J. Newman, J.M. Thummel, S.-P. Olesen, M. Grunnet, and E.M. Jorgensen. 2008. Single-copy insertion of transgenes in *Caenorhabditis elegans*. *Nat Genet*. 40:1375–1383. doi:10.1038/ng.248.

Galletta, B.J., C.J. Fagerstrom, T.A. Schoborg, T.A. McLamarrah, J.M. Ryniawec, D.W. Buster, K.C. Slep, G.C. Rogers, and N.M. Rusan. 2016. A centrosome interactome provides insight into organelle assembly and reveals a non-duplication role for Plk4. *Nature Communications*. 7:1–15. doi:10.1038/ncomms12476.

Garbrecht, J., T. Laos, E. Holzer, M. Dillinger, and A. Dammermann. 2021. An acentriolar centrosome at the *C. elegans* ciliary base. 1–32. doi:10.1016/j.cub.2021.03.023.

Hamill, D.R., A.F. Severson, J.C. Carter, and B. Bowerman. 2002. Centrosome maturation and mitotic spindle assembly in *C. elegans* require SPD-5, a protein with multiple coiled-coil domains. *Developmental Cell*. 3:673–684.

Hilbert, M., M.C. Erat, V. Hachet, P. Guichard, I.D. Blank, I. Flückiger, L. Slater, E.D. Lowe, G.N. Hatzopoulos, M.O. Steinmetz, P. Gönczy, and I. Vakonakis. 2013. *Caenorhabditis elegans* centriolar protein SAS-6 forms a spiral that is consistent with imparting a ninefold symmetry. *Proc. Natl. Acad. Sci. U.S.A.* 110:11373–11378. doi:10.1073/pnas.1302721110.

Kemp, C.A., K.R. Kopish, P. Zipperlen, J. Ahringer, and K.F. O'Connell. 2004. Centrosome maturation and duplication in *C. elegans* require the coiled-coil protein SPD-2. *Developmental Cell*. 6:511–523.

Kirkham, M., T. Müller-Reichert, K. Oegema, S. Grill, and A.A. Hyman. 2003. SAS-4 Is a *C. elegans* Centriolar Protein that Controls Centrosome Size. *Cell*. 112:575–587. doi:10.1016/s0092-8674(03)00117-x.

Kitagawa, D., I. Vakonakis, N. Olieric, M. Hilbert, D. Keller, V. Olieric, M. Bortfeld, M.C. Erat, I. Flückiger, P. Gönczy, and M.O. Steinmetz. 2011. Structural Basis of the 9-Fold Symmetry of Centrioles. *Cell*. 144:364–375. doi:10.1016/j.cell.2011.01.008.

Leidel, S., and P. Gönczy. 2003. SAS-4 is essential for centrosome duplication in *C. elegans* and is recruited to daughter centrioles once per cell cycle. *Developmental Cell*. 4:431–439.

Leidel, S., M. Delattre, L. Cerutti, K. Baumer, and P. Gönczy. 2005. SAS-6 defines a protein family required for centrosome duplication in *C. elegans* and in human cells. *Nature Cell Biology*. 7:115–125. doi:10.1038/ncb1220.

Lerit, D.A., H.A. Jordan, J.S. Poulton, C.J. Fagerstrom, B.J. Galletta, M. Peifer, and N.M. Rusan. 2015. Interphase centrosome organization by the PLP-Cnn scaffold is required for centrosome function. *The Journal of Cell Biology*. 210:79–97. doi:10.1083/jcb.201503117.

Lettman, M.M., Y.L. Wong, V. Viscardi, S. Niessen, S.-H. Chen, A.K. Shiau, H. Zhou, A. Desai, and K. Oegema. 2013. Direct Binding of SAS-6 to ZYG-1 Recruits SAS-6 to the Mother Centriole for Cartwheel Assembly. *Developmental Cell*. 25:284–298. doi:10.1016/j.devcel.2013.03.011.

Letunic, I., and P. Bork. 2018. 20 years of the SMART protein domain annotation resource. *Nucleic Acids Research*. 46:D493–D496. doi:10.1093/nar/gkx922.

Li, S., C.M. Armstrong, N. Bertin, H. Ge, S. Milstein, M. Boxem, P.-O. Vidalain, J.-D.J. Han, A. Chesneau, T. Hao, D.S. Goldberg, N. Li, M. Martinez, J.-F. Rual, P. Lamesch, L. Xu, M. Tewari, S.L. Wong, L.V. Zhang, G.F. Berriz, L. Jacotot, P. Vaglio, J. Reboul, T. Hirozane-Kishikawa, Q. Li, H.W. Gabel, A. Elewa, B. Baumgartner, D.J. Rose, H. Yu, S. Bosak, R. Sequerra, A. Fraser, S.E. Mango, W.M. Saxton, S. Strome, S. van den Heuvel, F. Piano, J. Vandenhaute, C. Sardet, M. Gerstein, L. Doucette-Stamm, K.C. Gunsalus, J.W. Harper, M.E. Cusick, F.P. Roth, D.E. Hill, and M. Vidal. 2004. A map of the interactome network of the metazoan *C. elegans*. *Science*. 303:540–543. doi:10.1126/science.1091403.

Lupas, A., Van Dyke, M., and Stock, J. 1991. Predicting Coiled Coils from Protein Sequences *Science* 252:1162-1164. DOI: 10.1126/science.252.5009.1162

Lupas, A. 1996. Prediction and Analysis of Coiled-Coil Structures *Meth. Enzymology* 266:513-525. DOI: 10.1016/s0076-6879(96)66032-7

Magescas, J., S. Eskinazi, M.V. Tran, and J.L. Feldman. 2021. Centriole-less pericentriolar material serves as a microtubule organizing center at the base of *C. elegans* sensory cilia. *Current Biology*. 1–24. doi:10.1016/j.cub.2021.03.022.

McNally, K.L.P., A.S. Fabritius, M.L. Ellefson, J.R. Flynn, J.A. Milan, and F.J. McNally. 2012. Kinesin-1 Prevents Capture of the Oocyte Meiotic Spindle by the Sperm Aster. *Developmental Cell*. 22:788–798. doi:10.1016/j.devcel.2012.01.010.

Mittasch, M., V.M. Tran, M.U. Rios, A.W. Fritsch, S.J. Enos, B. Ferreira Gomes, A. Bond, M. Kreysing, and J.B. Woodruff. 2020. Regulated changes in material properties underlie centrosome disassembly during mitotic exit. *The Journal of Cell Biology*. 219:647–23. doi:10.1083/jcb.201912036.

O'Connell, K.F., C. Caron, K.R. Kopish, D.D. Hurd, K.J. Kemphues, Y. Li, and J.G. White. 2001. The *C. elegans zyg-1* gene encodes a regulator of centrosome duplication with distinct maternal and paternal roles in the embryo. *Cell*. 105:547–558.

Pelletier, L., E. O'Toole, A. Schwager, A.A. Hyman, and T. Müller-Reichert. 2006. Centriole assembly in *Caenorhabditis elegans*. *Nature*. 444:619–623. doi:10.1038/nature05318.

Pelletier, L., N. Özlü, E. Hannak, C. Cowan, B. Habermann, M. Ruer, T. Müller-Reichert, and A.A. Hyman. 2004. The *Caenorhabditis elegans* Centrosomal Protein SPD-2 Is Required for both Pericentriolar Material Recruitment and Centriole Duplication. *Current Biology*. 14:863–873. doi:10.1016/j.cub.2004.04.012.

Qiao, R., G. Cabral, M.M. Lettman, A. Dammermann, and G. Dong. 2012. SAS-6 coiled-coil structure and interaction with SAS-5 suggest a regulatory mechanism in *C. elegans* centriole assembly. *EMBO J*. 1–14. doi:10.1038/emboj.2012.280.

R Core Team (2014). R: A language and environment for statistical computing. R Foundation for Statistical. Computing, Vienna, Austria. URL http://www.R-project.org/

Ren, J., L. Wen, X. Gao, C. Jin, Y. Xue, and X. Yao. 2009. DOG 1.0: illustrator of protein domain structures. *Cell Res.* 19:271–273. doi:10.1038/cr.2009.6.

Rogala, K.B., N.J. Dynes, G.N. Hatzopoulos, J. Yan, S.K. Pong, C.V. Robinson, C.M. Deane, P. Gönczy, and I. Vakonakis. 2015. The *Caenorhabditis elegans* protein SAS-5 forms large oligomeric assemblies critical for centriole formation. *eLife*. 4:e07410. doi:10.7554/eLife.07410.

Schindelin, J., I. Arganda-Carreras, E. Frise, V. Kaynig, M. Longair, T. Pietzsch, S. Preibisch, C. Rueden, S. Saalfeld, B. Schmid, J.-Y. Tinevez, D.J. White, V. Hartenstein, K. Eliceiri, P. Tomancak, and A. Cardona. 2012. Fiji: an open-source platform for biological-image analysis. *Nat Meth*. 9:676–682. doi:10.1038/nmeth.2019.

Schultz, J., R.R. Copley, T. Doerks, C.P. Ponting, and P. Bork. 2000. SMART: a web-based tool for the study of genetically mobile domains. *Nucleic Acids Research*. 28:231–234.

Sugioka, K., D.R. Hamill, J.B. Lowry, M.E. McNeely, M. Enrick, A.C. Richter, L.E. Kiebler, J.R. Priess, and B. Bowerman. 2017. Centriolar SAS-7 acts upstream of SPD-2 to regulate centriole assembly and pericentriolar material formation. *eLife*. 6:1–25. doi:10.7554/elife.20353.

Tinevez, J.-Y., N. Perry, J. Schindelin, G.M. Hoopes, G.D. Reynolds, E. Laplantine, S.Y. Bednarek, S.L. Shorte, and K.W. Eliceiri. 2017. TrackMate: An open and extensible platform for single-particle tracking. *Methods*. 115:80–90. doi:10.1016/j.ymeth.2016.09.016.

UniProt Consortium. 2019. UniProt: a worldwide hub of protein knowledge. *Nucleic Acids Research*. 47:D506–D515. doi:10.1093/nar/gky1049.

Uversky, V.N. 2019. Intrinsically Disordered Proteins and Their “Mysterious” (Meta)Physics. 1–18. doi:10.3389/fphy.2019.00010.

Varadarajan, R., and N.M. Rusan. 2018. Bridging centrioles and PCM in proper space and time. *Essays in Biochemistry*. 62:793–801. doi:10.1042/EBC20180036.

Woodruff, J.B., B.F. Gomes, P.O. Widlund, J. Mahamid, A. Honigmann, and A.A. Hyman. 2017. The Centrosome Is a Selective Condensate that Nucleates Microtubules by Concentrating Tubulin. *Cell*. 169:1066–1071.e10. doi:10.1016/j.cell.2017.05.028.

Woodruff, J.B., O. Wueseke, V. Viscardi, J. Mahamid, S.D. Ochoa, J. Bunkenborg, P.O. Widlund, A. Pozniakovsky, E. Zanin, S. Bahmanyar, A. Zinke, S.H. Hong, M. Decker, W. Baumeister, J.S. Andersen, K. Oegema, and A.A. Hyman. 2015. Regulated assembly of a supramolecular centrosome scaffold in vitro. *Science*. 348:808–812. doi:10.1126/science.aaa3923.

**FIGURES**

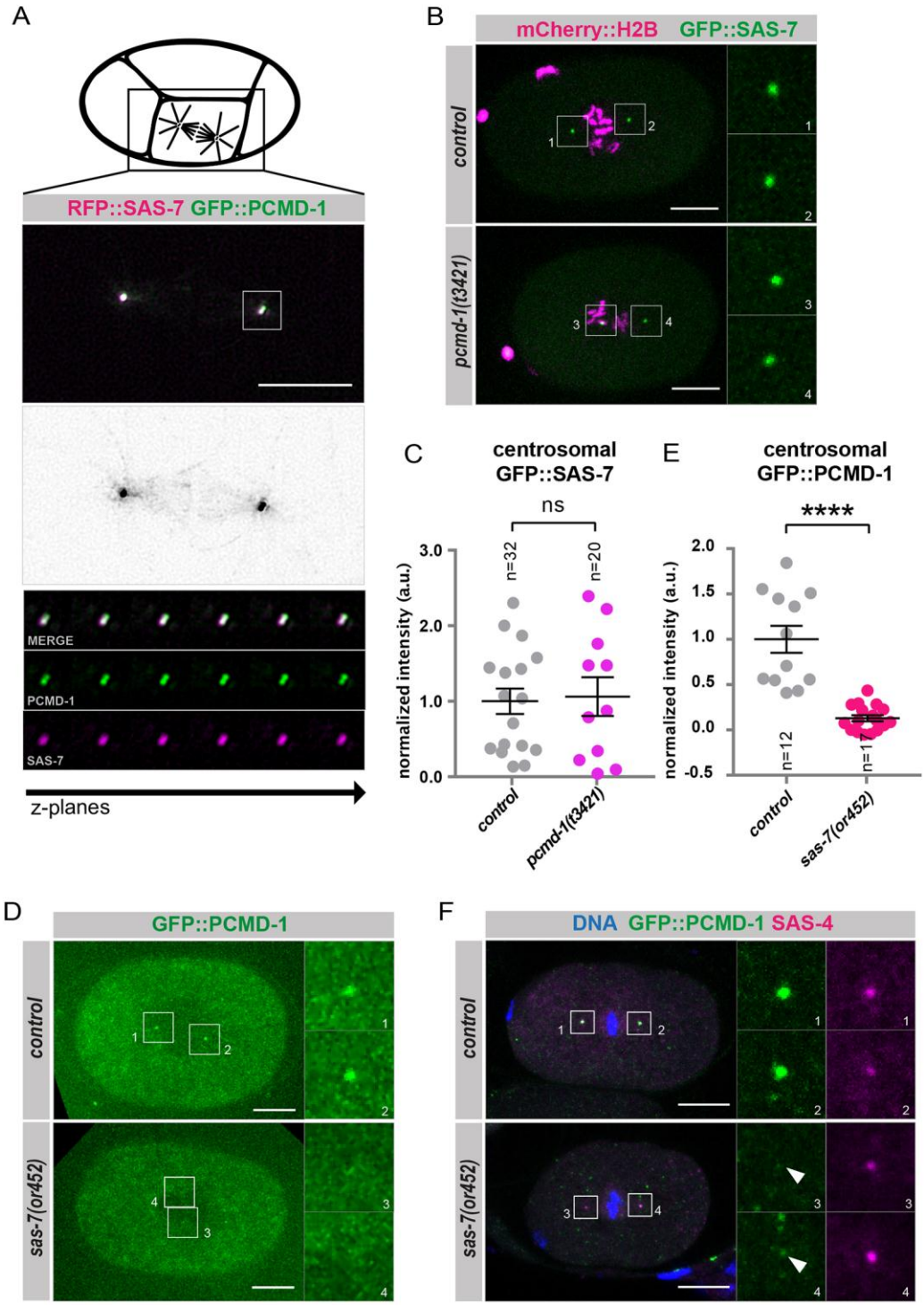


**Figure 1. SAS-7 recruits PCMD-1 to the centrioles**

(A) Mitotic centrosomes of the EMS cell of a 4-cell embryo (schematic) expressing GFP::PCMD-1 and RFP::SAS-7 (n=6 centrosomes). Note that some GFP signals decorated astral and kinetochore microtubules of the mitotic spindle (middle panel). Lower panels represent a montage of different Z-planes spanning a centriole pair.

(B) Stills of time-lapse spinning disc confocal images of *mCherry::h2b;gfp::sas-7* (n=16) and *pcmd-1(t3421);mCherry::h2b;gfp::sas-7* (n=10) embryos during nuclear envelope break-down (NEB). Insets represent centrosomes.
(C) Normalized centrosomal GFP::SAS-7 signal intensities in control and *pcmd-1(t3421)* mutant embryos at NEB. Two-sample t-test, n=number of analyzed centrosomes.
(D) Stills of time-lapse spinning disk confocal images of *gfp::pcmd-1* (n=6) and *gfp::pcmd-1;sas-7(or452)* (n=10) embryos during pronuclear meeting. Centrosomal areas are shown enlarged for the GFP::PCMD-1 signal.
(E) Normalized centrosomal GFP::PCMD-1 signal intensities in control and *sas-7(or452)* embryos at NEB. Two-sample t-test, n=number of analyzed centrosomes.
(F) Representative confocal images of fixed *gfp::pcmd-1* (n=8) and *gfp::pcmd-1;sas-7(or452)* (n=11) one-cell embryos in prometaphase stained for DNA, GFP and SAS-4. Insets represent single channels of the centrioles. Arrowheads indicate for the GFP::PCMD-1 signal.
In all panels error bars denote s.e.m. p-values represent ****$p<0.0001$, ns $p>0.05$. In all panels, scale bars are 10 μm.

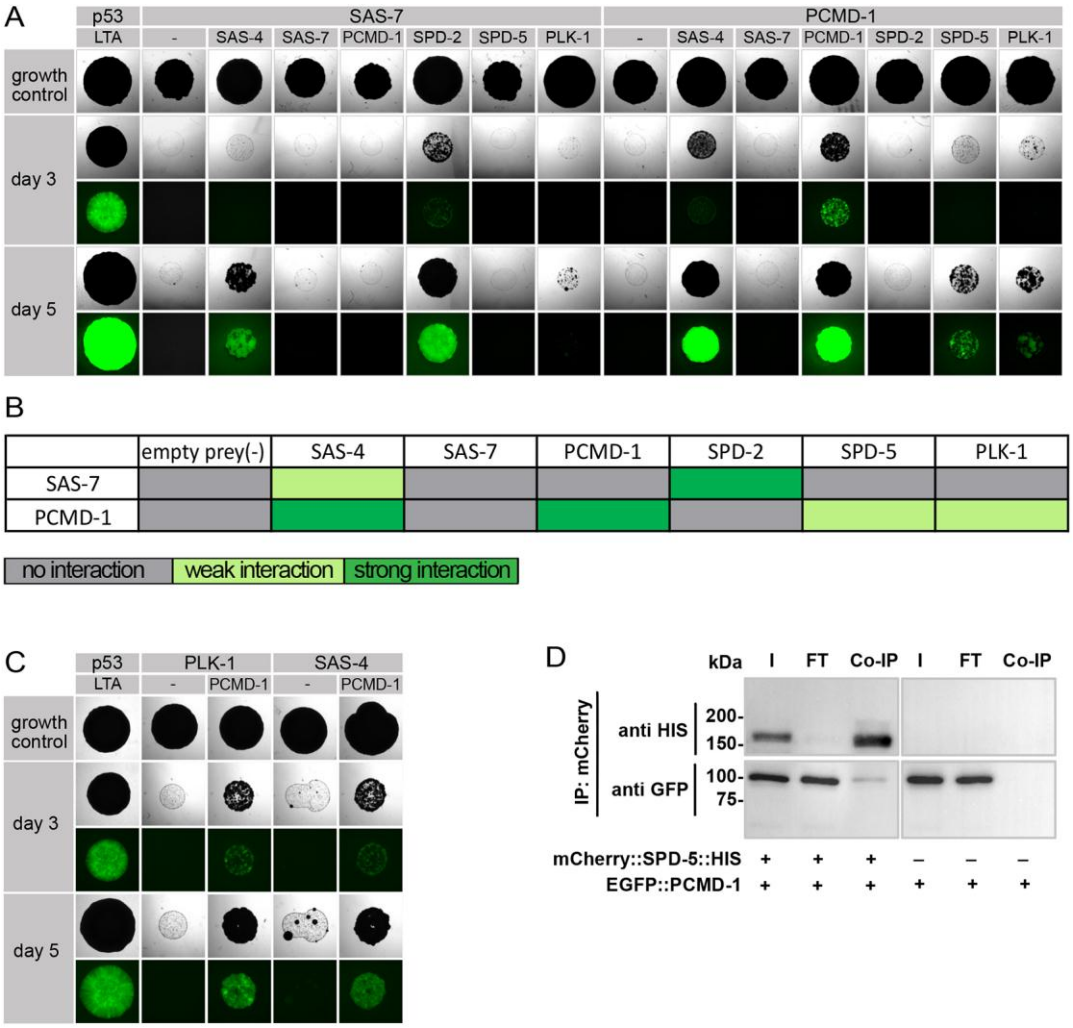


**Figure 2. PCMD-1 interacts with centriolar and PCM scaffold proteins**

(A) Images of representative yeast two-hybrid colonies. Interaction of bait proteins SAS-7 and PCMD-1 with centrosomal proteins SAS-7, SAS-4, PCMD-1, SPD-2, SPD-5, and PLK-1 as preys, respectively. The top panel represents growth control, middle panels represent colonies screened on day 3 for growth on the selection medium and expression of the GFP-reporter, and the bottom panels represent colonies screened on day 5 for growth on the selection medium and expression of the GFP-reporter.

(B) Summary of protein-protein interactions observed categorized by the strength of their interactions.

(C) Images of representative yeast two-hybrid colonies. Interaction of bait proteins PLK-1 and SAS-4 with PCMD-1 prey.

(D) Co-immunoprecipitation of *C. elegans* EGFP::PCMD-1 and mCherry::SPD-5::6xHIS expressed in HEK293T cells using an RFP-trap. I represents the input fraction, FT represents the flow-through, Co-IP is Co-immunoprecipitation.

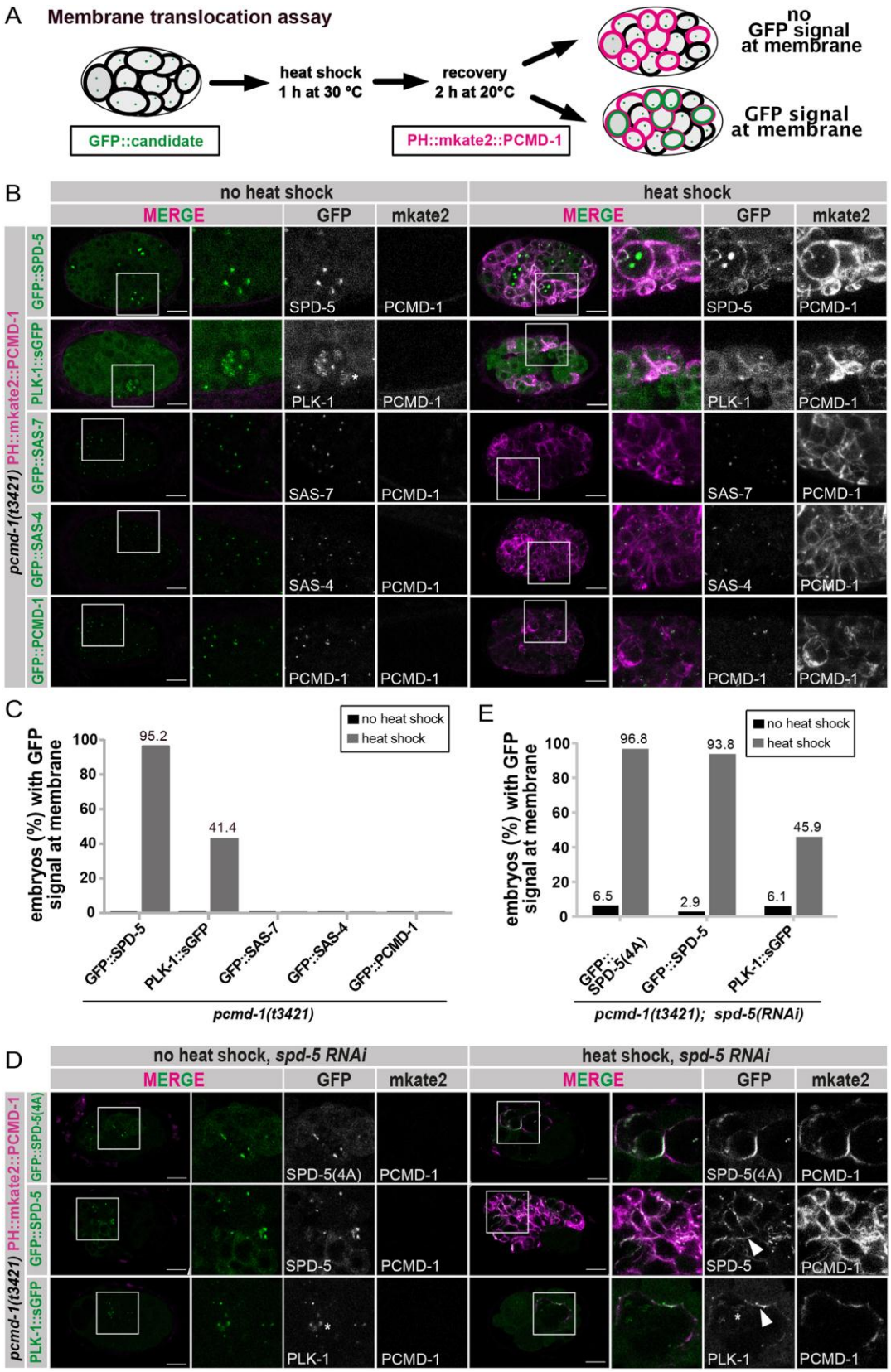


**Figure 3. PCMD-1 targets SPD-5 and PLK-1 to the plasma membrane**

(A) Schematic representation of the 'translocation assay'. After 1h heat shock to induce expression and 2h recovery, PH::mkate2::PCMD-1 is expressed and binds to the plasma membrane of a multicellular embryo. If PH::mkate2::PCMD-1 recruits GFP-tagged candidate

proteins, they will also localize to the plasma membrane (bottom embryo). If PH::mkate2::PCMD-1 is not able to recruit, the localization of the GFP-tagged candidate proteins will not change upon PH::mkate2::PCMD-1 expression (top embryo).
(B) Representative multicellular embryos of the 'translocations assay' for GFP::SPD-5 (n=17 no heat shock; n=21 heat shock), PLK-1::sGFP (n=21 no heat shock; n=29 heat shock), GFP::SAS-7 (n=20 no heat shock; n=23 heat shock), GFP::SAS-4 (n=28 no heat shock; n=28 heat shock) and GFP::PCMD-1 (n=25 no heat shock; n=27 heat shock) fusion proteins in the *pcmd-1(t3421)* background with and without heat shock. Selected regions are enlarged and shown as merge and single channels. Note that PLK-1::sGFP signal at the plasma membrane is less intense than GFP::SPD-5. Scale bars are 10 μm.
(C) Quantification of (B); percentage of embryos (%) with GFP signal at the membrane after heat shock in the *pcmd-1(t3421)* background.
(D) Representative multicellular embryos of the 'translocations assay' using GFP::SPD-5 (n=31 no heat shock; n=31 heat shock), GFP::SPD-5(4A) (n=34 no heat shock; n=32 heat shock), and PLK-1::sGFP (n=33 no heat shock; n=37 heat shock) in a *pcmd-1(t3421);spd-5(RNAi)* background. Selected regions are enlarged and shown as merge and single channels. Arrowheads indicate the membrane-localized GFP signal. Asterisk indicated kinetochore localization of PLK-1::sGFP. Scale bars are 10 μm.
(E) Quantification of (D); percentage of embryos (%) with GFP signal at the membrane after heat shock in the *pcmd-1(t3421); spd-5(RNAi)* background.

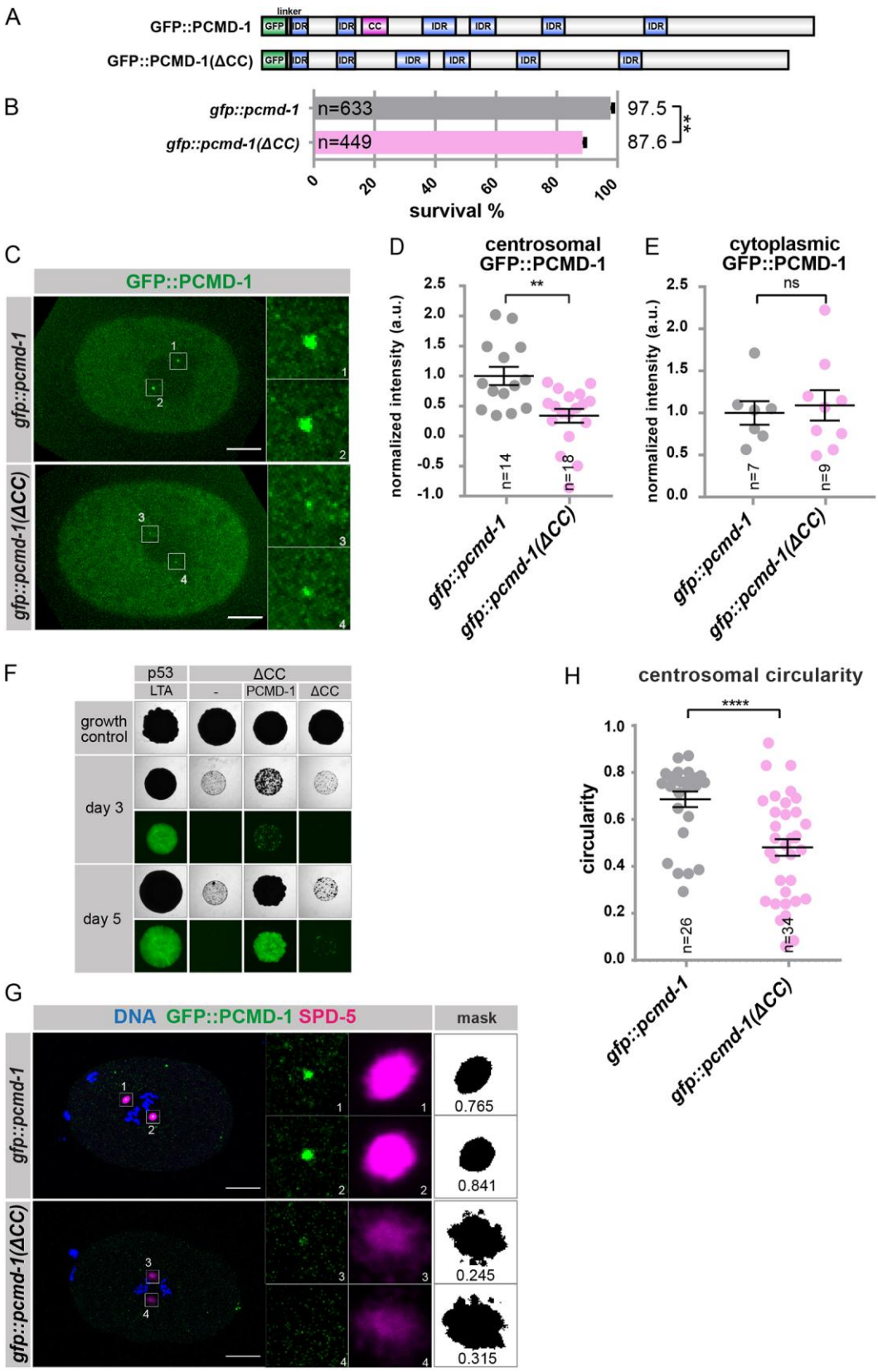


**Figure 4. The coiled-coil domain promotes PCMD-1 accumulation at the centrosome and PCM scaffold integrity**

(A) Schematic representation of the domain structure of endogenously tagged GFP::PCMD-1 protein (aa 2-630), with predictions of the coiled-coil domain (CC) and six Intrinsically

Disordered Regions (IDRs) (top). Schematic representation of the domain structure of a truncated version, with the deleted coiled-coil domain (Δ86-117). All domains except GFP are represented to the relative scale.
(B) Survival (%) of *gfp::pcmd-1* and *gfp::pcmd-1(ΔCC)* animals at 25°C. p-values were calculated by Mann-Whitney-U Test, n=number of analyzed embryos.
(C) Stills of time-lapse imaging of *gfp::pcmd-1* (n=7) and *gfp::pcmd-1(ΔCC)* (n=9) embryos at NEB. Centrosomal areas were determined by DIC imaging and are shown enlarged for the GFP::PCMD-1 signal. See movies 1 and 2.
(D) Normalized centrosomal GFP signal intensities in embryos expressing *gfp::pcmd-1* and *gfp::pcmd-1(ΔCC)* at NEB. p-values were calculated by Mann-Whitney-U test. n=number of analyzed centrosomes.
(E) Normalized cytoplasmic GFP signal intensities in embryos expressing *gfp::pcmd-1* and *gfp::pcmd-1(ΔCC)* at NEB. p-values were calculated by two-sample t-test. n=number of analyzed embryos.
(F) Images of representative yeast two-hybrid colonies. Interaction of bait proteins PCMD-1(ΔCC) with PCMD-1 and PCMD-1(ΔCC) as preys.
(G) Representative images of fixed embryos of the indicated genotype stained for DNA, GFP and SPD-5. Enlarged are centrosomes in individual channels and the corresponding masks of the SPD-5 signal. Indicated are the values of centrosomal circularity.
(H) Quantification of SPD-5 circularity in *gfp::pcmd-1* and *gfp::pcmd-1(ΔCC)* embryos. p-values were calculated by Mann-Whitney-U Test, n=number of analyzed centrosomes.
In all panels error bars denote s.e.m. p-values represent **p<0.01, ****p<0.0001, ns p>0.05. Scale bars are 10 μm.

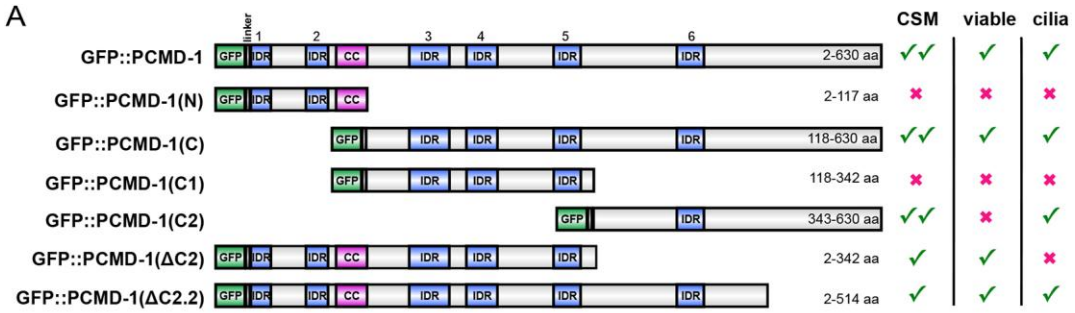


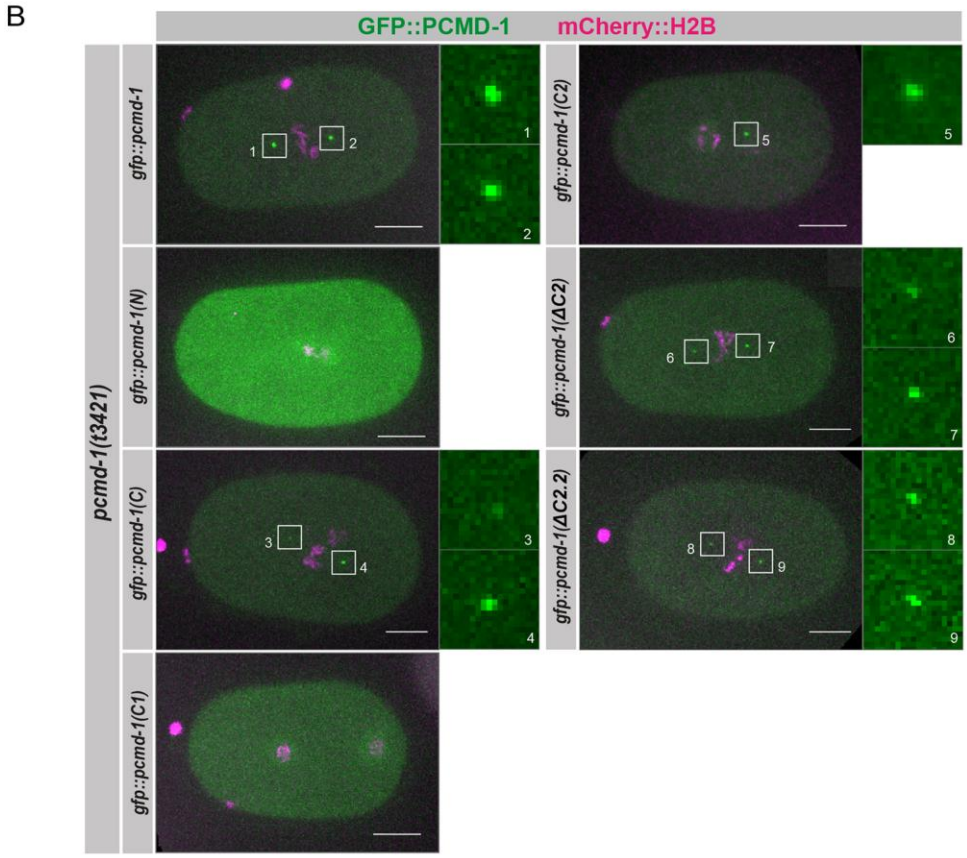


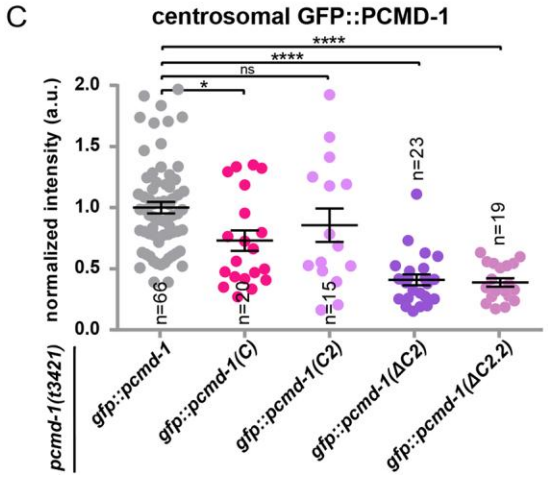


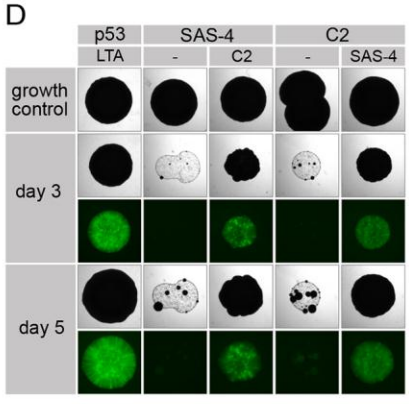

**Figure 5. The C-terminal region targets PCMD-1 to the centrosome and binds SAS-4**

(A) Domain structure of different GFP-tagged PCMD-1 constructs. All domains except GFP are represented to the relative scale. All constructs are expressed under the regulatory elements of the *mai-2* gene. Summary of localization and viability. CSM = centrosome

(B) Stills of time-lapse imaging of embryos expressing *gfp::pcmd-1* (n=12), *gfp::pcmd-1(N)* (n=7), *gfp::pcmd-1(C)* (n=10), *gfp::pcmd-1(C1)* (n=8), *gfp::pcmd-1(C2)* (n=9), *gfp::pcmd-1(ΔC2)* (n=12) and *gfp::pcmd-1(ΔC2.2)* (n=10) in combination with the *mCherry::h2b* in the *pcmd-1(t3421)* background at NEB. Enlarged are the two centrosomes. n=number of embryos.

(C) Normalized centrosomal GFP signal intensities of embryos represented in (B). P-values were determined with Multiple Comparison with Kruskal Wallis test and post-hoc Dunn's test adjusted with Holm correction, n=number of analyzed centrosomes.

(D) Images of representative yeast two-hybrid colonies. Interaction of bait proteins SAS-4 and PCMD-1(C2) with SAS-4 and PCMD-1(C2) as preys.

In all panels error bars denote s.e.m. p-values represent * $p<0.05$, **** $p<0.0001$, ns $p>0.05$. Scale bars are 10 μm.

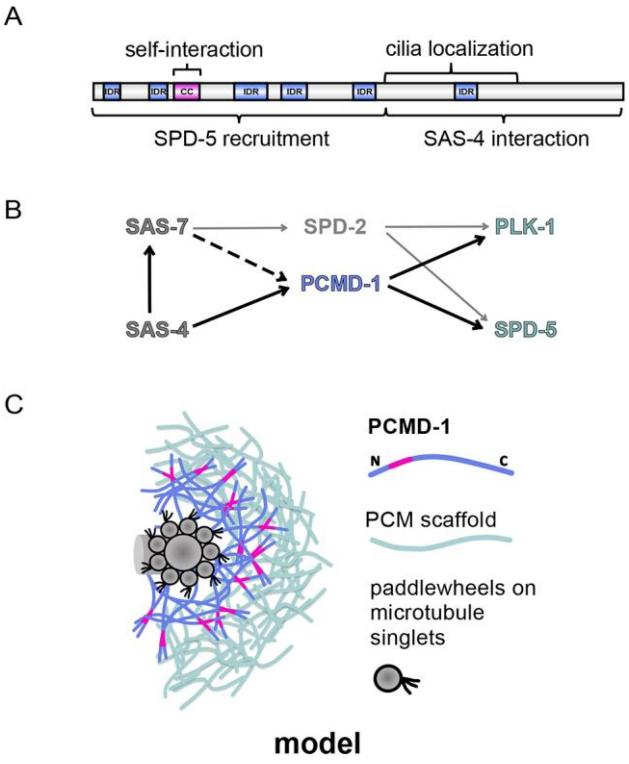


**Figure 6. Model of how PCMD-1 bridges the centrioles and PCM**

(A) Structure of PCMD-1 with the indicated interaction sites

(B) Genetic interactions of PCMD-1. Interactions identified in this study are indicated by black arrows. PCMD-1 is genetically downstream of SAS-7 and SAS-4. SAS-7 itself interacts with SAS-4 and SPD-2. PCMD-1 acts genetically upstream of SPD-5 and PLK-1. Proteins other than PCMD-1, as SPD-2 are involved in SPD-5 and PLK-1 recruitment to the centrosome.

(C) Proposed model: PCMD-1 interacts with both centriolar and PCM proteins and thereby bridges the two centrosomal components. PCMD-1 is tethered to the centrioles through its C-terminal part, while the N-terminal part, including the coiled-coil domain, plays a role in PCMD-1 self-interaction and PCM formation.

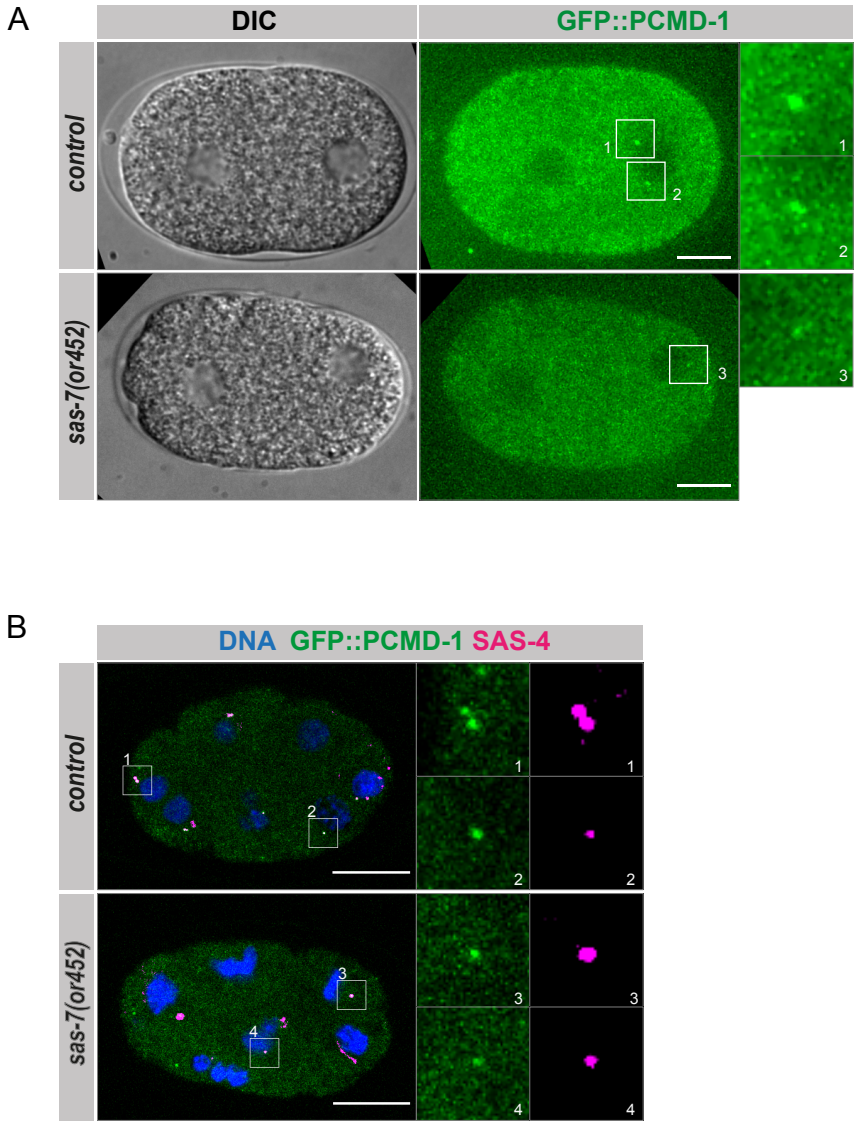


**Fig. S1. SAS-7 recruits PCMD-1 to the centrioles in early embryos**
(A) Stills of time-lapse spinning disc confocal images of *gfp::pcmd-1* (n=6) and *gfp::pcmd-1;sas-7(or452)* (n=8) embryos during pronuclear migration. Centrosomes are shown enlarged for the GFP::PCMD-1 signal.
(B) Representative confocal images of fixed *gfp::pcmd-1* (n=3) and *gfp::pcmd-1;sas-7(or452)* (n=8) embryos (>6 nuclei) stained for DNA, GFP and SAS-4. Insets represent single channels of the centrioles.
In all panels, scale bars are 10 μm.

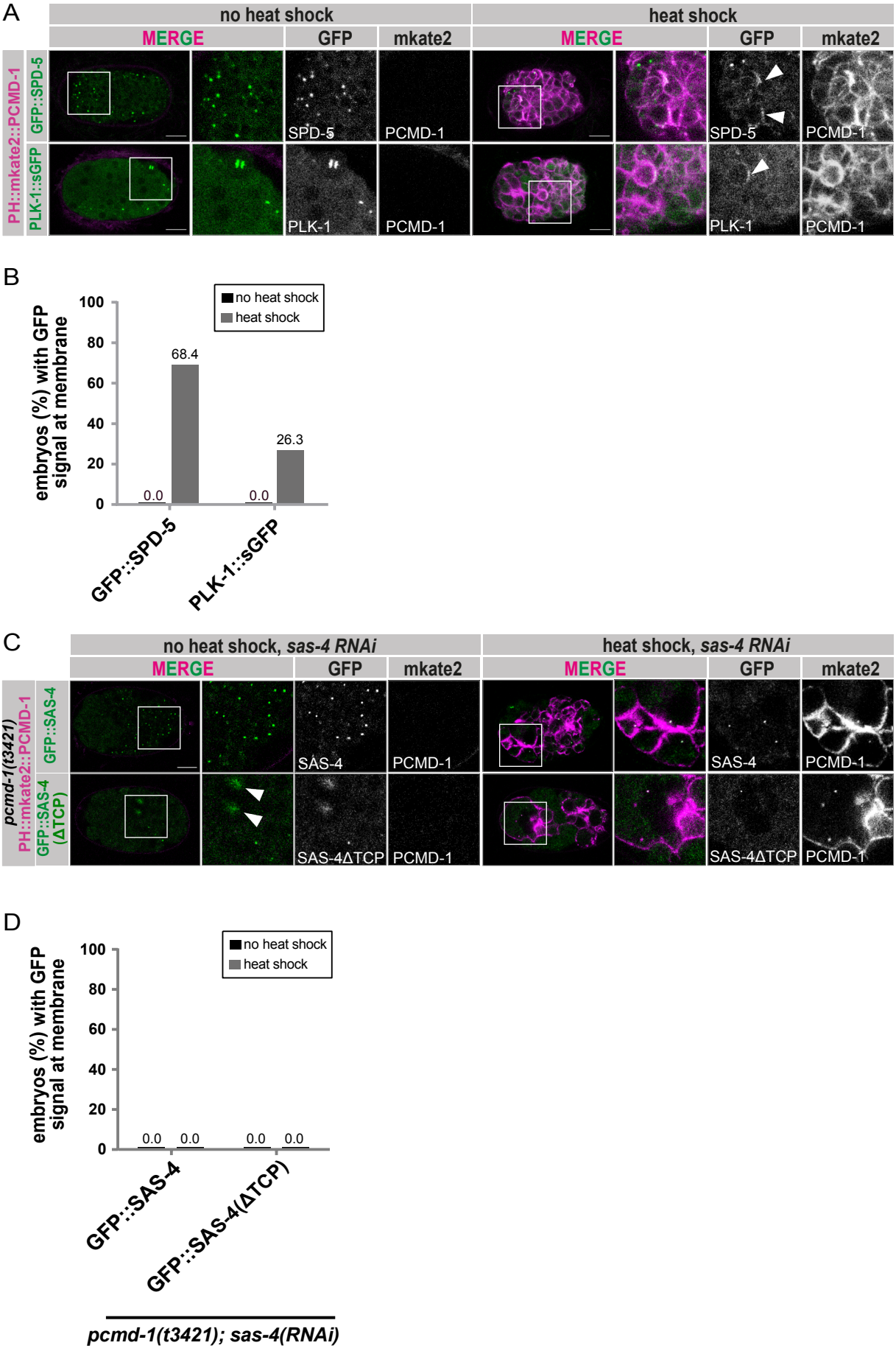

**Fig. S2. PCMD-1 targeting of SPD-5 and PLK-1 to the plasma membrane in the presence of endogenous PCMD-1 is less efficient**

(A) Representative multicellular embryos of the 'translocations assay' using GFP::SPD-5 (n=19 no heat shock; n=19 heat shock), and PLK-1::sGFP (n=20 no heat shock; n=19 heat shock) in a wild-type background. Selected regions are enlarged and shown as merge and single channels. Note that plasma membrane-localized PLK-1::sGFP is faint. Scale bars are 10 µm.

(B) Quantification of (A); the percentage of embryos (%) with GFP signal at the membrane after heat shock in the wild-type background.

(C) Representative multicellular embryos of the 'translocations assay' using GFP::SAS-4 (n=33 no heat shock; n=36 heat shock), and GFP::SAS-4(deltaTCP) (n=30 no heat shock; n=29 heat shock) in a *pcmd-1(t3421)* background and treated with *sas-4(RNAi)*. Selected regions are enlarged and shown as merge and single channels. Scale bars are 10 µm.

(D) Quantification of (C); the percentage of embryos (%) with GFP signal at the membrane after heat shock in the *sas-4(RNAi)* background.

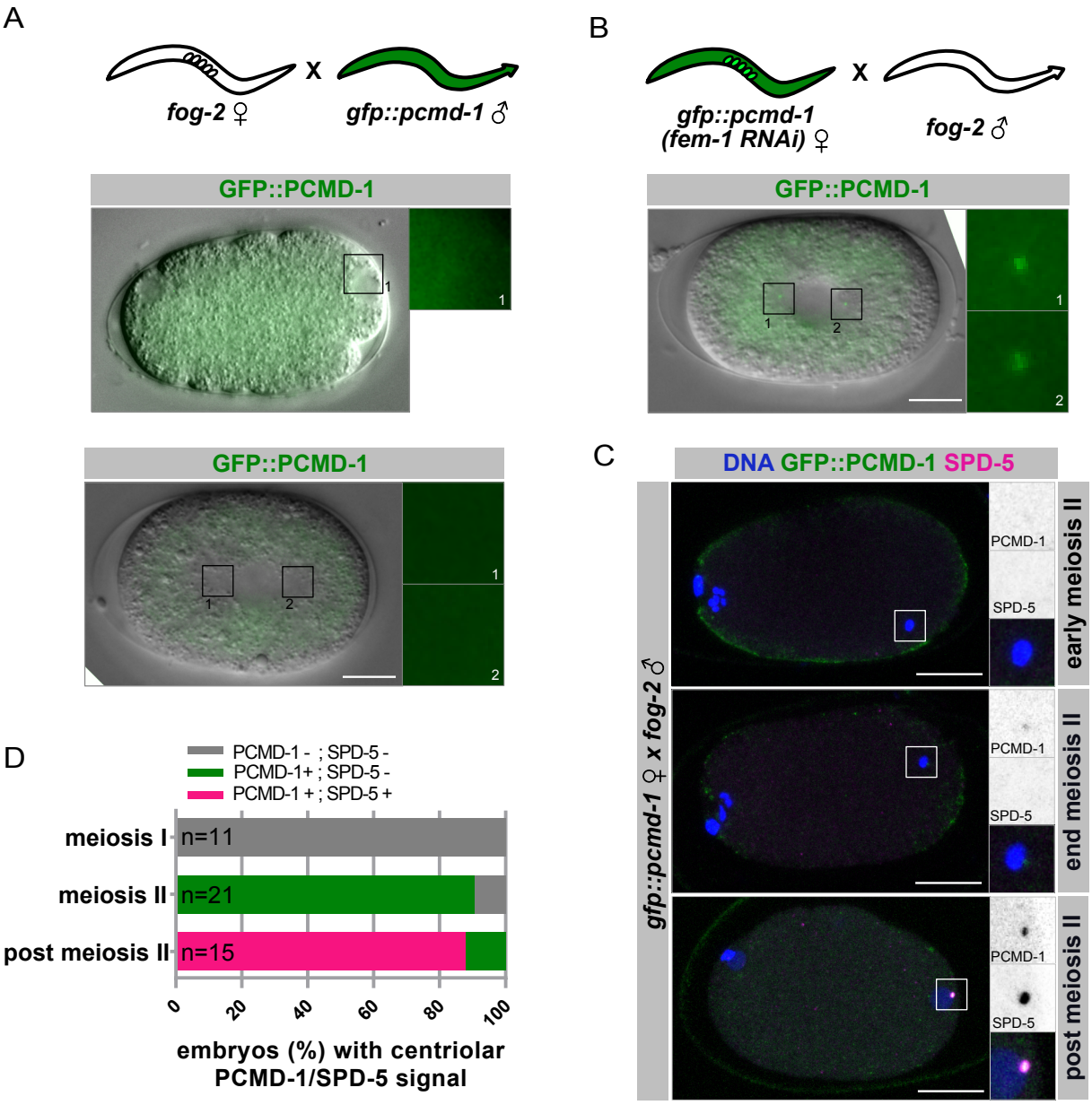


**Fig. S3. PCMD-1 is recruited before SPD-5 to sperm-derived centrioles**
(A) Schematic representation of a marked mating experiment where *fog-2(n71)* females were mated with *gfp::pcmd-1* males. The images below represent one-cell embryos taken by live-cell imaging shortly after meiosis II (n=6) and at metaphase (n=11). Centrosomal areas were determined by DIC imaging and are shown enlarged for the GFP::PCMD-1 signal.
(B) Schematic representation of a marked mating experiment where *fem-1(RNAi)*-treated *gfp::pcmd-1* females were mated with *fog-2(n71)* males (n=10). The image below represents a one-cell embryo taken by live-cell imaging. Centrosomal areas were determined by DIC imaging and are shown enlarged for the GFP::PCMD-1 signal.
(C) Images of fixed embryos in different stages of meiosis II, derived from the cross indicated in (B) and stained for DNA, GFP and SPD-5. Enlarged are sperm-associated centrosomal signals merged and as single channels.
(D) Quantification of (C) percentage of embryos (%).
Scale bars in all panels are 10 µm.

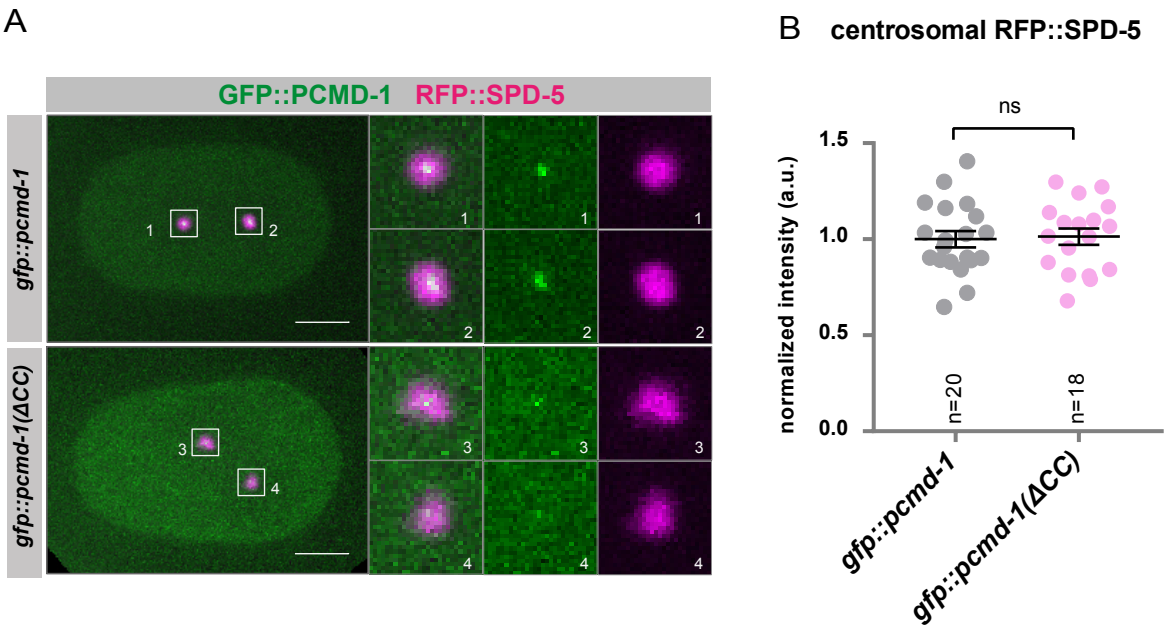


**Fig. S4. Deletion of the coiled-coil domain PCMD-1 does not affect centrosomal SPD-5 levels**
(A) Stills of time-lapse imaging of embryos expressing *rfp::spd-5 gfp::pcmd-1* (n=10) and *rfp::spd-5 gfp::pcmd-1(deltaCC)* (n=9) at metaphase. Centrosomal areas are shown enlarged as merge and for the RFP::SPD-5, GFP::PCMD-1 signal. n=number of embryos.
(B) Normalized centrosomal RFP signal intensities in embryos expressing *rfp::spd-5 gfp::pcmd- 1* and *rfp::spd-5 gfp::pcmd-1(deltaCC)* at metaphase. Two Sample t-test. n=number of analyzed centrosomes. ns $p>0.05$. Scale bars are 10 µm.

A

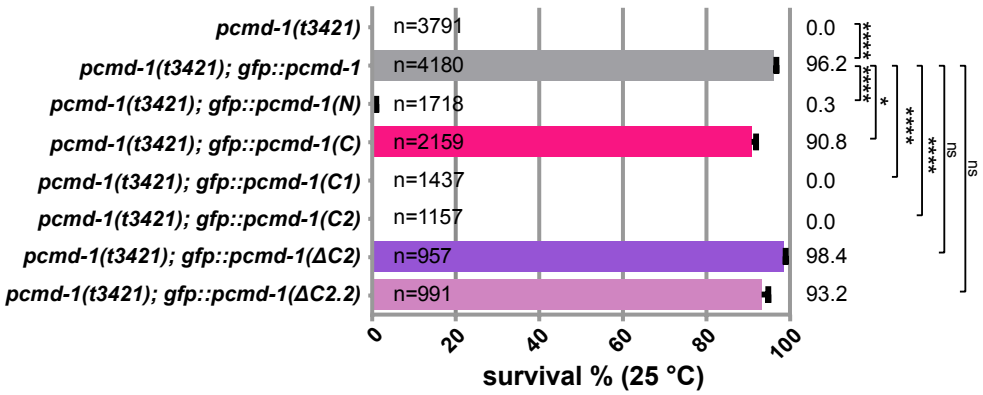


B

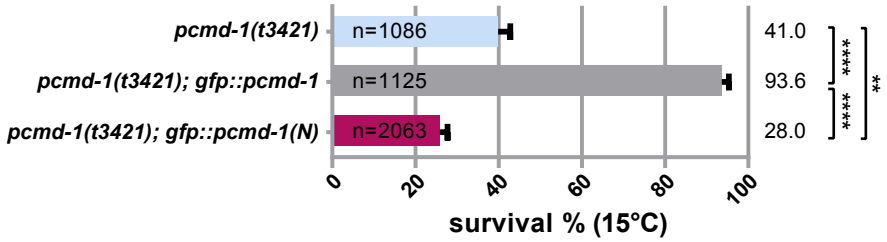


C

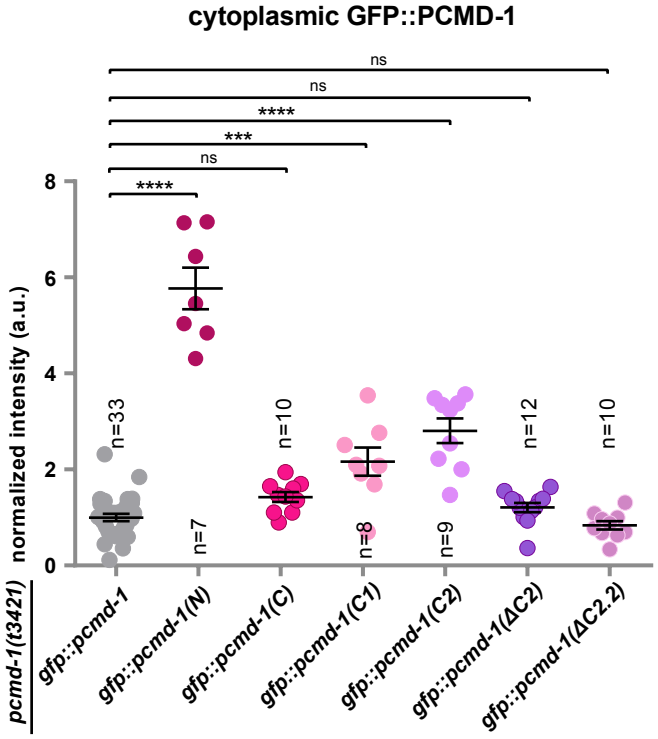

D

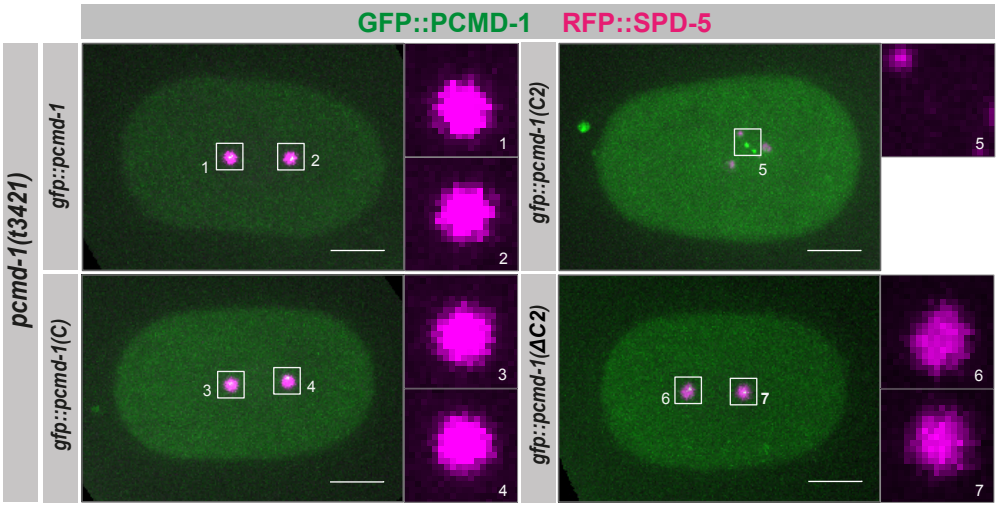


E

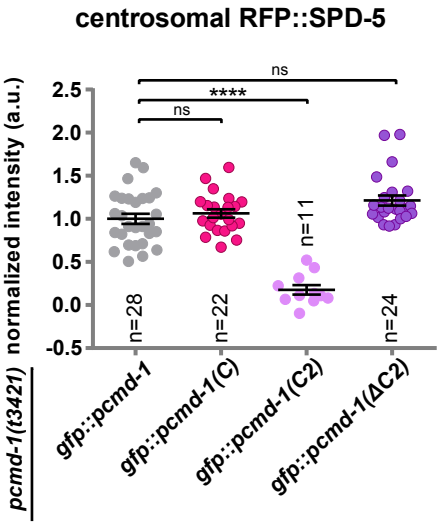


**Fig. S5. The C2-region of PCMD-1 is insufficient to recruit SPD-5 to the centrosome**

(A) Survival (%) of *gfp::pcmd-1, gfp::pcmd-1(N), gfp::pcmd-1(C), gfp::pcmd-1(C1), gfp::pcmd-1(C2), gfp::pcmd-1(deltaC2)* and *gfp::pcmd-1(deltaC2.2)* in the *pcmd-1(t3421)* background at 25C. Multiple Comparison with Kruskal Wallis test and post-hoc Dunn's test adjusted with Holm correction. n=number of analyzed embryos.

(B) Survival (%) of *gfp::pcmd-1* and *gfp::pcmd-1(N)* embryos in the *pcmd-1(t3421)* background at 15C. P-values were determined with multiple Comparison with Kruskal Wallis test and post-hoc Dunn's test adjusted with Holm correction, n=number of analyzed embryos.

(C) Normalized cytoplasmic GFP signal intensities of *gfp::pcmd-1, gfp::pcmd-1(N), gfp::pcmd-1(C), gfp::pcmd-1(C1), gfp::pcmd-1(C2), gfp::pcmd-1(deltaC2)* and *gfp::pcmd-1(deltaC2.2)* embryos, in combination with the *mCherry::h2b* in the *pcmd-1(t3421)* background at NEB. P-values were determined with multiple Comparison with Kruskal Wallis test and post-hoc Dunn's test adjusted with Holm correction, n=number of analyzed embryos.

(D) Stills of time-lapse imaging of *rfp::spd-5; gfp::pcmd-1* (n=14) and *rfp::spd-5; gfp::pcmd-1(C)* (n=11), *rfp::spd-5; gfp::pcmd-1(C2)* (n=9) and *rfp::spd-5; gfp::pcmd-1(deltaC2)* (n=12) of embryos in the *pcmd-1(t3421)* background at metaphase. Note that in two *rfp::spd-5; gfp::pcmd-1(C2) embryos* the PCM does not co-localize with the centrioles. Centrosomal areas are shown enlarged as merge and for the RFP::SPD-5, GFP::PCMD-1 signal. n=number of embryos.

(E) Normalized centrosomal RFP::SPD-5 signal intensities at metaphase of embryos in (D). p-values were determined with Multiple Comparison with Kruskal Wallis test and post-hoc Dunn's test adjusted with Holm correction, n=number of analyzed centrosomes.

In all panels error bars denote s.e.m. p-values represent: **p<0.01, ***p<0.001, ****p<0.0001, ns p>0.05. Scale bars are 10 µm.

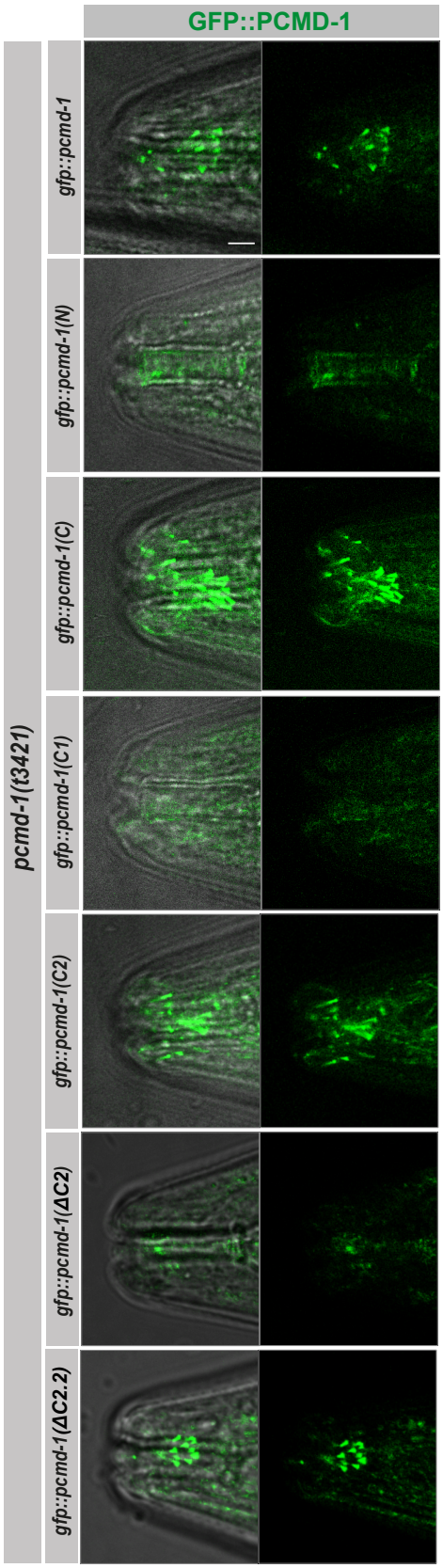


**Fig. S6. The region spanning the IDR6 is necessary for ciliary targeting of PCMD-1**
Localization of GFP::PCMD-1, GFP::PCMD-1(N), GFP::PCMD-1(C), GFP::PCMD-1(C1), GFP::PCMD-1(C2), GFP::PCMD-1(deltaC2) and GFP::PCMD-1(deltaC2.2) to the ciliary base in adult animals. n=5 animals for each condition.
Scale bars are 10 µm.

**Table S1.**

Click here to download Table S1

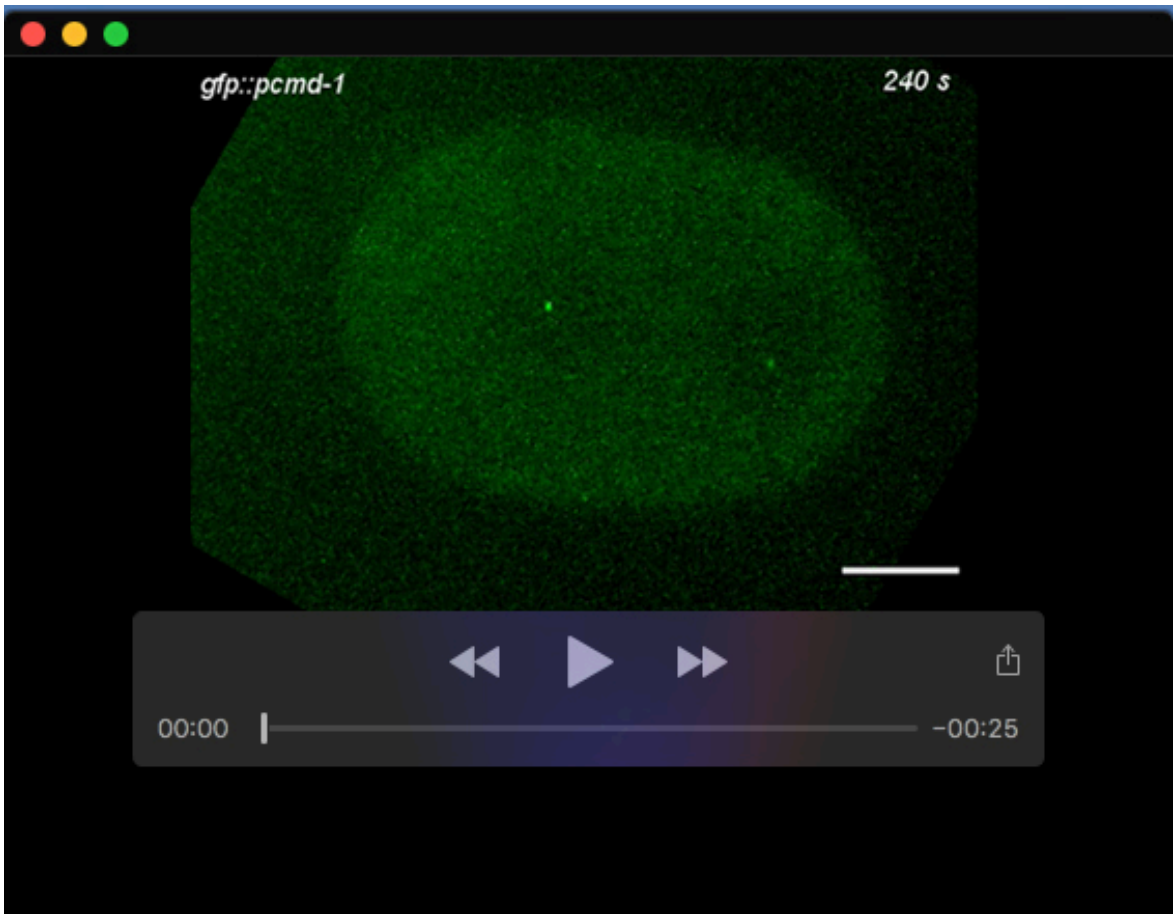


**Movie 1. Time-lapse of the first cell cycle of a GFP::PCMD-1 expressing embryo**
(related to figure 4C)
In the control embryo, GFP::PCMD-1 localizes to the centrosome throughout the first cell cycle. Live-cell spinning disk microscopy. The scale bar is 10 μm.

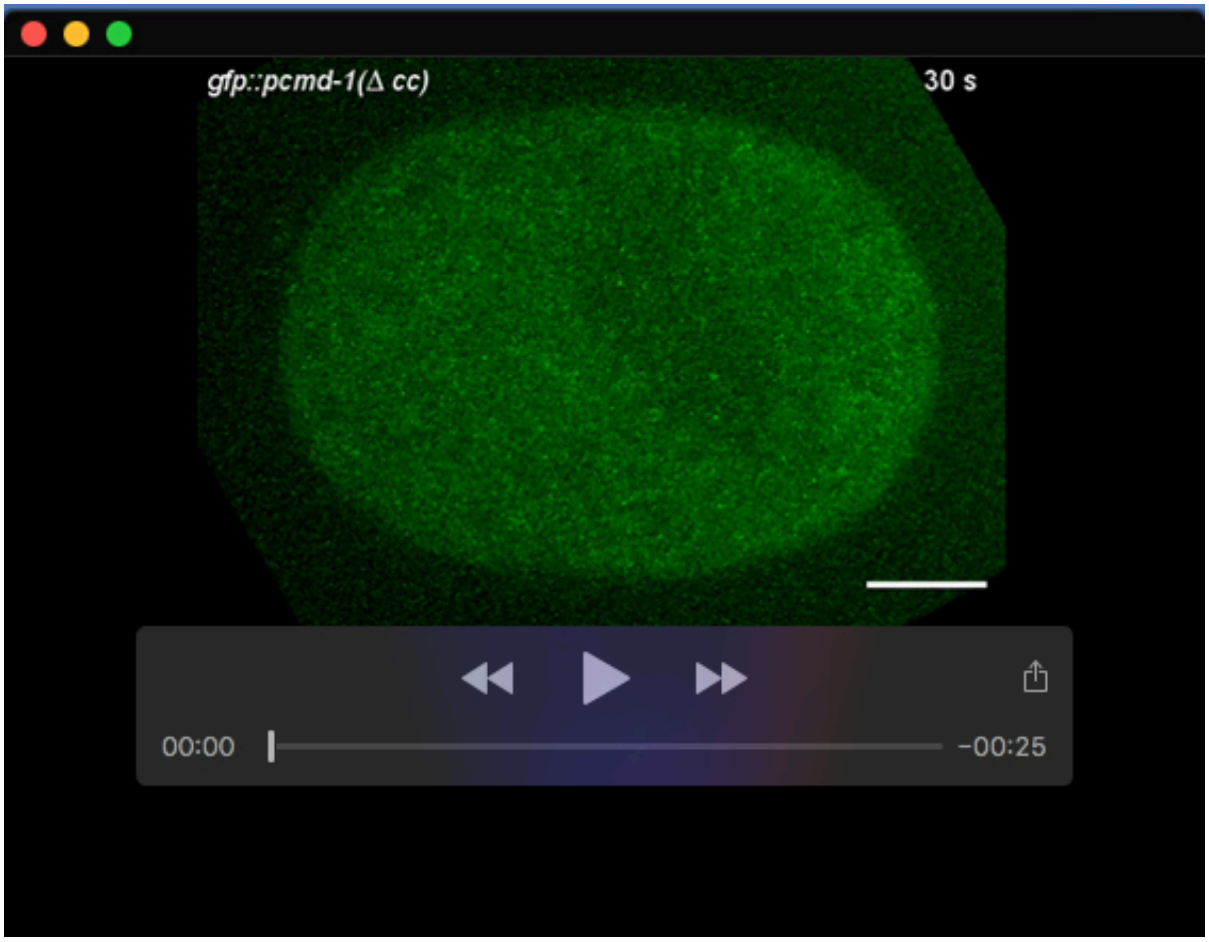


**Movie 2. Time-lapse of the first cell cycle of a GFP::PCMD-1 expressing embryo lacking the predicted coiled-coil domain** (related to figure 4C)
In the *gfp::pcmd-1(ΔCC)* embryo, GFP::PCMD-1(ΔCC) localizes to the centrosome with reduced levels. Live-cell spinning disk microscopy. The scale bar is 10 μm.